Earth Surface Processes and Landforms
Earth Surf. Process. Landforms **28**, 273–298 (2003)
Published online in Wiley InterScience (www.interscience.wiley.com). DOI: 10.1002/esp.485

CHANGES IN GEOMETRY AND SUBGLACIAL DRAINAGE OF MIDRE LOVÉNBREEN, SVALBARD, DETERMINED FROM DIGITAL ELEVATION MODELS

DAVID RIPPIN,[1]* IAN WILLIS,[1] NEIL ARNOLD,[1] ANDREW HODSON,[2] JOHN MOORE,[3] JACK KOHLER[4] AND HELGI BJÖRNSSON[5]

[1] *Scott Polar Research Institute and Department of Geography, University of Cambridge, Cambridge, CB2 1ER, UK*
[2] *Department of Geography, University of Sheffield, Winter Street, Sheffield, S10 2TN, UK*
[3] *Arctic Centre, University of Lapland, Box 122, 96101 Rovaniemi, Finland*
[4] *Norwegian Polar Institute, Polar Environmental Centre, N-9296, Tromsø, Norway*
[5] *Science Institute, University of Iceland, Dunhaga 3, IS-107 Reykjavik, Iceland*

Received 1 April 2001; Revised 19 May 2002; Accepted 1 June 2002

ABSTRACT

Digital elevation models (DEMs) of the bed and surface of the polythermal Midre Lovénbreen, Svalbard, are used to identify changes in glacier geometry between 1977 and 1995. The calculated mean annual mass balance ($-0{\cdot}61$ m water equivalent (w.e.) a^{-1}) is more negative than that derived from field measurements ($-0{\cdot}35$ m w.e. a^{-1}), although the error associated with this value ($\pm 0{\cdot}7$ m a^{-1}) suggests that the difference may be accounted for by errors. However, similar discrepancies between DEM-based and field-based measurements of mass balance have been reported elsewhere in Svalbard. Although errors may be responsible, patterns of surface elevation change may also be explained in terms of patterns of ablation, accumulation, and dynamics. The theoretical structure of the subglacial drainage system is modelled using different assumptions about subglacial water pressure, in 1977 and 1995. These reconstructions are compared with the observed positions of proglacial outlet streams. Decreasing subglacial water pressure results in a decrease in the influence of surface morphology and an increase in the role of the bed topography on drainage routing, which generally leads to more dispersed drainage. Long-term changes in the position of proglacial outlet streams occur as a result of changes in glacier geometry, but short-term changes may also occur in response to early season water pressures, controlled by meteorological and hydrological conditions. Copyright © 2003 John Wiley & Sons, Ltd.

KEY WORDS: digital elevation models; polythermal glacier; Svalbard; subglacial drainage; mass balance

INTRODUCTION

The study of glacier geometry and subglacial drainage is important for scientific reasons since both control glacier dynamics (Nye, 1957; Lliboutry, 1968; Iken, 1981; Hanson, 1995; Hubbard *et al*., 1998) and surge behaviour (Clarke *et al*., 1984; Kamb *et al*., 1985; Björnsson, 1998; Jiskoot *et al*., 2000). It is also important for practical reasons since changes in glacier geometry and drainage have important implications for glacier mass balance and sea level rise (Houghton *et al*., 2001) and runoff regimes in glacierized catchments (Benis-ton *et al*., 1997). Many field-based studies have provided detailed knowledge of the geometry and hydrology of specific glaciers and their changes over time (Bindschadler *et al*., 1977; Clarke and Blake, 1991; Fountain, 1993; Heinrichs *et al*., 1996; Iken and Truffer, 1997; Nienow *et al*., 1998). However, there is an increas-ing need to monitor glacier changes in many parts of the world without recourse to expensive field-based campaigns. For this reason, increasing use is being made of remote sensing and digital elevation modelling techniques. In particular, changes in glacier geometry can now readily be determined from the analysis of digital elevation models (DEMs) derived from sequential aerial photographs (Reinhardt and Rentsch, 1986; Etzelmüller *et al*., 1993; Willis *et al*., 1998; Kaab and Funk, 1999; Hubbard *et al*., 2000). Similarly, DEMs of glacier surfaces and beds may be used to calculate theoretical patterns of hydraulic potential across glacier

* Correspondence to: D. Rippin, Bristol Glaciology Centre, School of Geographical Sciences, University of Bristol, University Road, Bristol, BS8 1SS, UK. E-mail: d.m.rippin@bristol.ac.uk

beds (Shreve, 1972). These may then be used to identify the likely locations of subglacial drainage catchments, preferential drainage axes, and their change through time (Björnsson, 1988; Holmlund, 1988; Sharp *et al*., 1993; Fountain and Vaughn, 1995; Flowers and Clarke, 1999; Copland and Sharp, 2000; Hagen *et al*., 2000).

In this paper, we use DEM techniques to study the changes in geometry and subglacial drainage structure of Midre Lovénbreen, a small polythermal glacier in northwest Spitsbergen. It is particularly important to study the geometry and hydrology of these Arctic polythermal glaciers for three main reasons. First, while much is known about the hydrology of temperate glaciers, much less is known about that of polythermal glaciers (Tranter *et al*., 1996; Hodgkins, 1997). In particular, it is not fully understood how the water beneath the warm-based core of many polythermal glaciers penetrates the cold-based regions around their snout and margins (Wadham *et al*., 1998; Skidmore and Sharp, 1999). Second, polythermal glaciers are likely to be better analogues than temperate glaciers for the Pleistocene mid-latitude ice sheets (Sugden, 1977; Denton and Hughes, 1981; Arnold and Sharp, 1992; Heine and McTigue, 1996). Third, many climate modelling studies suggest that the Arctic will be the first region to experience climate changes in response to CO_2 induced global warming, and that these changes will be more marked than elsewhere (Stouffer *et al*., 1989; Walsh, 1991; Cattle and Crossley, 1995; Fleming *et al*., 1997). In particular, Spitsbergen, at 77–80 °N, 10–22 °E, is located at the northern extremity of the North Atlantic Drift, and so glaciers there may be particularly sensitive to, and good first indicators of, changing climate (Dowdeswell and Drewry, 1989; Fleming *et al*., 1997; Lefauconnier *et al*., 1999). Spitsbergen has already undergone a 4–5 °C increase in mean annual temperatures since the Little Ice Age early in the 20th century (Fleming *et al*., 1997). Climate changes may manifest themselves in polythermal glaciers not only as changes in ice thickness and extent, and the supply of water, but also as changes in the distribution of cold and temperate ice, which itself will impact upon water storage and routing, and thus ice dynamics.

The two main purposes of this paper are as follows.

1. To derive surface DEMs of Midre Lovénbreen in 1977 and 1995; use these to identify and explain patterns of surface elevation change and glacier mass balance; and compare the mass balance estimate with that derived from ground-based measurements made over the same time period.
2. To produce a bed DEM; couple this to the 1977 and 1995 surface DEMs; calculate the theoretical patterns of hydraulic potential beneath the glacier for various assumptions about the steady-state water pressure regime; calculate the likely locations of subglacial drainage catchments, preferential drainage axes, and their change through time; and compare these theoretical reconstructions with field observations of glacier hydrology to identify the likely steady-state water pressure regime beneath the glacier and how this may have changed through time.

FIELD SITE

Midre Lovénbreen (78·53 °N and 12·04 °E) is an alpine-type valley-glacier in northwest Spitsbergen (Figure 1). Below 50 m a.s.l., the mean annual temperature of west Spitsbergen is between −4·3 and −5·0 °C and precipitation ranges from 180 to 440 mm a^{-1} (Hanssen-Bauer *et al*., 1990; Hodson *et al*., 2000). Midre Lovénbreen consists of a western basin, southern basin and three small eastern basins that combine to feed the main glacier tongue (Figure 1). The glacier is *c*. 6 km long, with an area of *c*. 5·5 km^2 and a maximum thickness of *c*. 180 m (Björnsson *et al*., 1996). It ranges in elevation from *c*. 50 m a.s.l. at the snout to *c*. 600 m a.s.l. at the headwall. Its equilibrium line altitude (ELA) averages *c*. 395 m a.s.l. and its accumulation area ratio (AAR) averages *c*. 0·35 (Björnsson *et al*., 1996). The glacier is polythermal with a warm-based core, cold-based ice around its snout and margins, and cold ice at its surface (Hagen and Sætrang, 1991; Ødegård *et al*., 1992, Björnsson *et al*., 1996), although the winter cold-wave is eliminated in the accumulation basins (Björnsson *et al*., 1996). Mass balance measurements have been made at a series of stakes along the glacier centreline since 1967 by the Norsk Polarinstitutt (Figure 1).

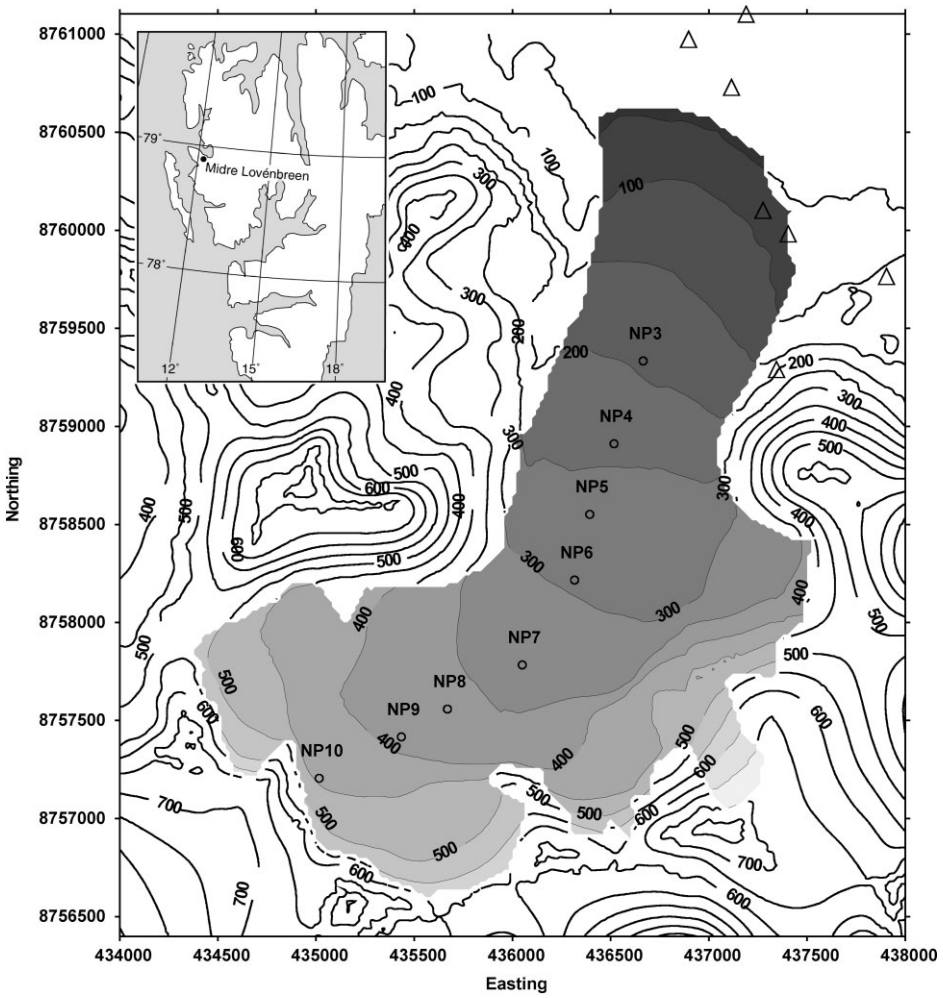

Figure 1. Midre Lovénbreen with Norsk Polarinstitutt ablation stakes (open circles) and photogrammetric reference points (open triangles) marked. Map based on 1979 Norsk Polarinstitutt 1 : 20 000 map of *Brøggerbreane, Vestre og Midre Lovénbreen* (based on data collected in 1977). Contours in metres. North is to top of figure. The 400 m contour approximates the mean ELA at *c*. 395 m a.s.l. Two photogrammetric reference points appear to be located on the glacier surface. In 1999, the glacier had retreated so that these reference points were not located on the glacier. Inset shows the location of Midre Lovénbreen in Spitsbergen

METHODOLOGY

Bed elevation data

Bed elevation data were derived using ground-penetrating radar (GPR) on two separate occasions. The first data-set was collected in May 1990 (Björnsson *et al*., 1996). The bed reflection was detected using a radar system operating at 5–20 MHz. The system was sledge-mounted and pulled by a skidoo. Measurements were taken every 4·2 or 8·4 m. The system was positioned with reference to a terrestrially surveyed glacier surface grid used for mass-balance measurements to a horizontal accuracy of *c*. 5 m. The data-set consisted of 450 data points. The accuracy of the GPR measurements can be assessed by comparing the GPR depths measured at the mass balance stakes 3 and 9 with depths determined by drilling at these sites in 1990 (Figure 1). GPR-derived depths were *c*. 126 m and *c*. 135 m at stakes 3 and 9 respectively while drill depths were respectively *c*. 122 m and *c*. 133 m suggesting errors of $< \pm 5$ m. However, overall bed elevation errors were determined from a full consideration of the properties of the radar system and the accuracy with which its position was known at any time, and were estimated to be ± 15 m (Björnsson *et al*., 1996).

The second GPR data-set was collected using a 50 MHz radar system in May 1998 (Moore, unpublished data). The data-set consisted of *c*. 5000 points, collected while the sledge-mounted system was pulled behind a skidoo. The system was positioned using a global positioning system to a horizontal accuracy of *c*. 1 m. Data were recorded at fixed time intervals of 0·5 s, which equated to one trace every *c*. 1–3 m. Bed elevation errors were again determined from a full consideration of the properties of the radar system and its positioning, and were estimated to be ±5 m.

Between them, the 1990 and 1998 bed data-sets consist of three longitudinal profiles along the eastern half, western half, and centreline of the glacier, and a series of approximately transverse profiles that zigzag back and forth across the glacier (Figure 2). The data-sets cover similar areas and cover most of the glacier although data from the upper basins could not be obtained due to deep snow, steep slopes and crevasses. Before combining these two data-sets, collected by different workers using different equipment and at different times, we assessed the extent to which they were comparable.

To obtain a large data-set for comparison, and accounting for the errors associated with fixing the positions of the GPR points, we compared depth data from the two data-sets for points that were collected within a

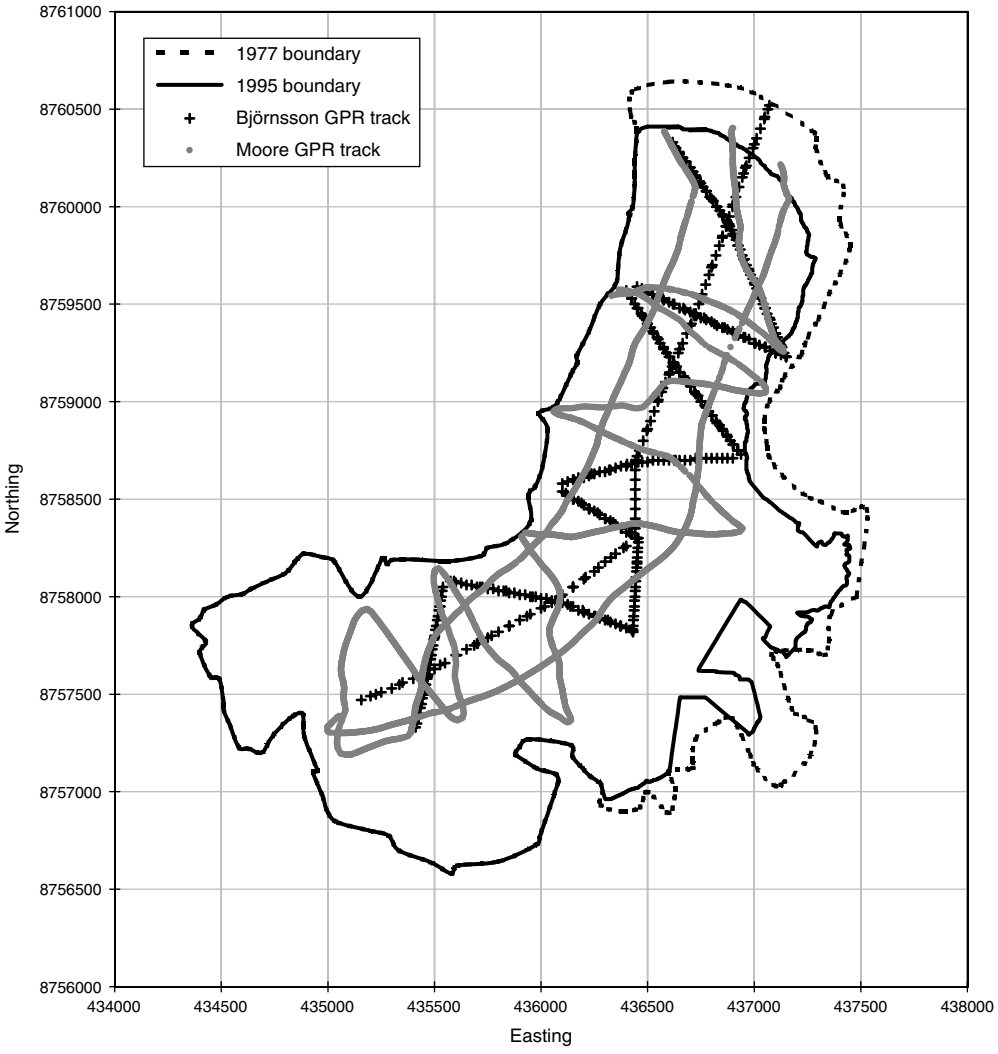

Figure 2. Glacier boundaries (1977 and 1995) and GPR tracks taken by H. Björnsson in 1990 and J. Moore in 1998

horizontal distance of 10 m of one another. This produced 322 comparable data points, although, because of the higher resolution of the 1998 data-set, there are occasions when one 1990 point may be compared with more than one 1998 point.

There is a very good correlation between the two data-sets ($R^2 = 0{\cdot}99$) and the relationship between them is very close to one-to-one (Figure 3). The maximum difference in bed elevation between the two data-sets is 21·35 m and the minimum difference is 1·16 m. On average, the 1998 bed elevations are greater than the 1990 elevations but the mean difference between the two data-sets is only 7·19 m and the mean absolute difference is only 10·23 m. As the mean absolute difference is within the bed elevation errors of 15 m for the 1990 data-set, the two bed elevation data-sets were considered comparable and were therefore combined to produce a bed DEM as described below.

Surface elevation data

Surface elevation data were also available from two sources. In the first case, data were derived from the Norsk Polarinstitutt 1 : 20 000 map entitled *Brøggerbreane, Vestre og Midre Lovénbreen*, published in 1979, but derived from aerial photographs taken in 1977. This map was digitized using ArcInfo. Errors were determined from a consideration of errors in the original map, and from errors inherent in the digitizing technique, and were estimated to be ±5 m in the horizontal and ±10 m in the vertical.

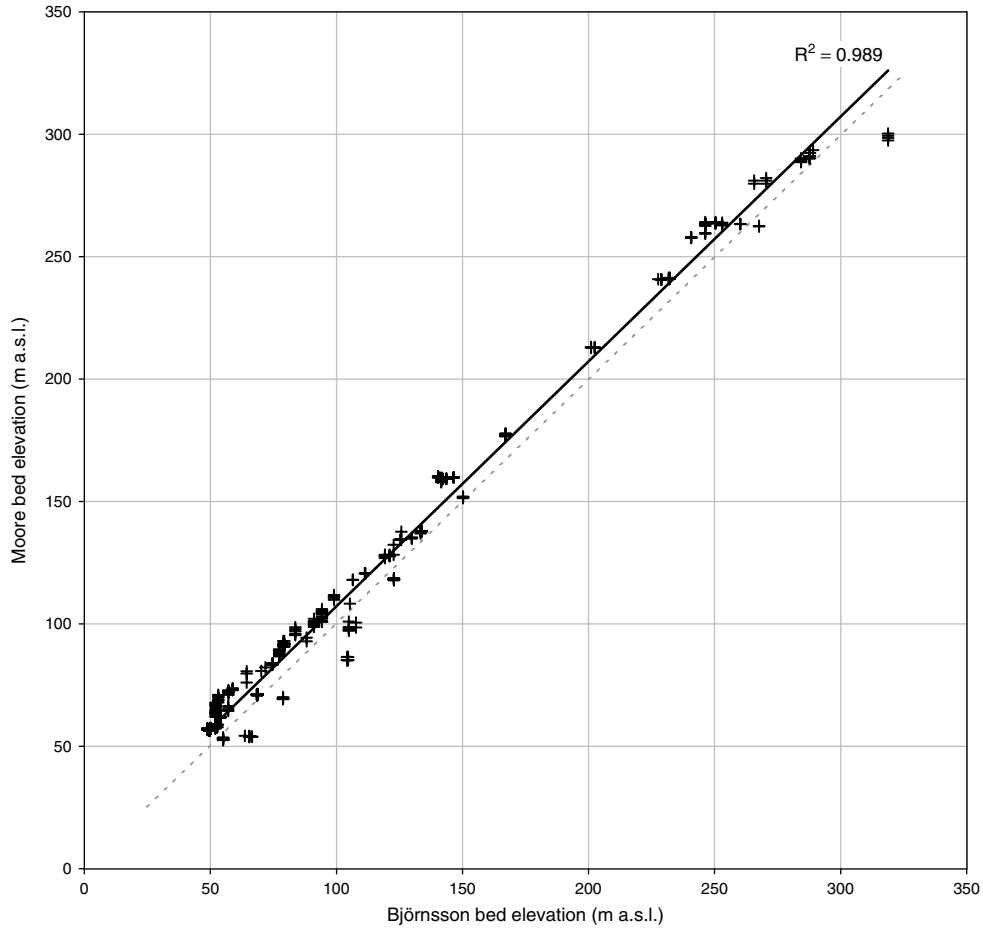

Figure 3. Comparison of raw Björnsson and Moore bed elevation data where points are within 10 m of one another. The dotted line is an idealized 1 : 1 fit between the two data-sets, while the black line is the best-fit between the available data

A second surface elevation data-set was derived using analytical photogrammetry from six stereo-overlapping aerial photographs taken in August 1995, supplied by the Norsk Polarinstitutt (images S95 1069–1071 and S95 1081–1083). The technique converted the x, y coordinates of points within the stereo-images to three-dimensional x, y, z coordinates. The first stage of the process used a number of the points identifiable on each image to establish the relative geometric relationship between each pair of images (Dixon *et al.*, 1998). The stereo-model was then orientated with respect to the UTM coordinate system. This stage required ground control points, i.e. points on the ground for which horizontal and vertical coordinates were known, and which were clearly visible on both images of a stereo pair. Seven such ground control points were surveyed during the summer of 1999 using a Geodimeter Total Station from two fixed stations on the western valley side with reference to two fixed points to the east. A least-squares adjustment was used to fix the coordinates of each point from multiple surveys. These points were fixed into the UTM system with reference to hand-held GPS measurements. Due to problems of accessibility and safety, all seven control points had to be located in the glacier forefield (Figure 1).

The lack of ground control points higher up the catchment was potentially problematic in terms of accurately positioning the entire glacier model within the UTM coordinate system. We attempted to compensate for this deficit by accurately fixing the overlap between the images of the upper glacier with a large number of tie-points (i.e. features visible on both images of a pair). In this way, the three-dimensional glacier model was more internally consistent and could be translated into the UTM coordinate system based on the few ground control points with greater confidence (Dixon *et al.*, 1998). Data were initially gridded onto a 3·5 m regular grid where topography was visible. A few areas of shadow, particularly to the west and south, and a few areas of 'featureless' snow cover in the upper basins prevented the topography from being determined in these regions.

To test the accuracy of the 1995 surface elevation data, grid cells within the provisional 3·5 m DEM were compared with the GPS-derived surface elevation data measured during the 1998 GPR survey. Some discrepancy between the data-sets is to be expected, as they were collected three years apart, and because there was a widespread, thick snowcover during the GPR survey in May, but a limited, thin snowcover in the aerial photographs taken in August. Nevertheless, it was considered that this comparison would provide a useful check on the accuracy of the provisional 1995 DEM, especially since ground-based measurements in 1995 were not made. A total of 663 points distributed across the glacier were selected from the original 1998 GPR data-set. Any cells in the provisional 1995 DEM that were within a horizontal distance of 10 m of a GPR point were used for comparison. The 10 m distance was used because of likely errors in the positioning of points between the two data-sets. This created 18 399 comparable data points.

A plot of the comparable data points is shown in Figure 4. Below *c*. 240 m a.s.l. there is a well-defined linear relationship between the two data-sets although the GPR points are slightly higher than the equivalent provisional DEM cells. Above *c*. 240 m a.s.l. there is more scatter in the relationship between the two data-sets. Some provisional DEM cells are lower than the equivalent GPR points and some are higher. This suggests that below *c*. 240 m a.s.l., the provisional DEM has been precisely defined but is slightly inaccurate owing to a systematic error. Above *c*. 240 m a.s.l. the provisional DEM is both imprecise and inaccurate. This presumably reflects the concentration of ground control points near to the glacier snout but the lack of control points surrounding the upper glacier. To account for the systematic error and render the provisional DEM more accurate, a linear regression equation was fitted to the data below 240 m (Figure 4). This equation was used to correct the provisional DEM data. The effect of this 'tuning' was to raise the 1995 photogrammetrically derived data up to the level of the 1998 GPS-derived data. The mean absolute difference between all the GPR elevations and the uncorrected DEM elevations was 23·2 m (14·1 m below 240 m a.s.l.; 32·1 m above 240 m a.s.l.), while after the correction, this difference was reduced to 9·8 m (2·0 m below 240 m a.s.l.; 17·3 m above 240 m a.s.l.), and thus mean surface elevation errors in 1995 were approximately the same as in 1977. It is recognized that this procedure will not eliminate the imprecision on the upper glacier.

Creation of digital elevation models (DEMs)

The combined irregularly spaced bedrock topography data-sets, the contoured surface elevation data-set from 1977, and the corrected provisional 3·5 m gridded surface DEM from 1995 (with gaps), were each interpolated onto regular 20 × 20 m grids using the rubber-sheeting interpolation procedure in ERDAS IMAGINE

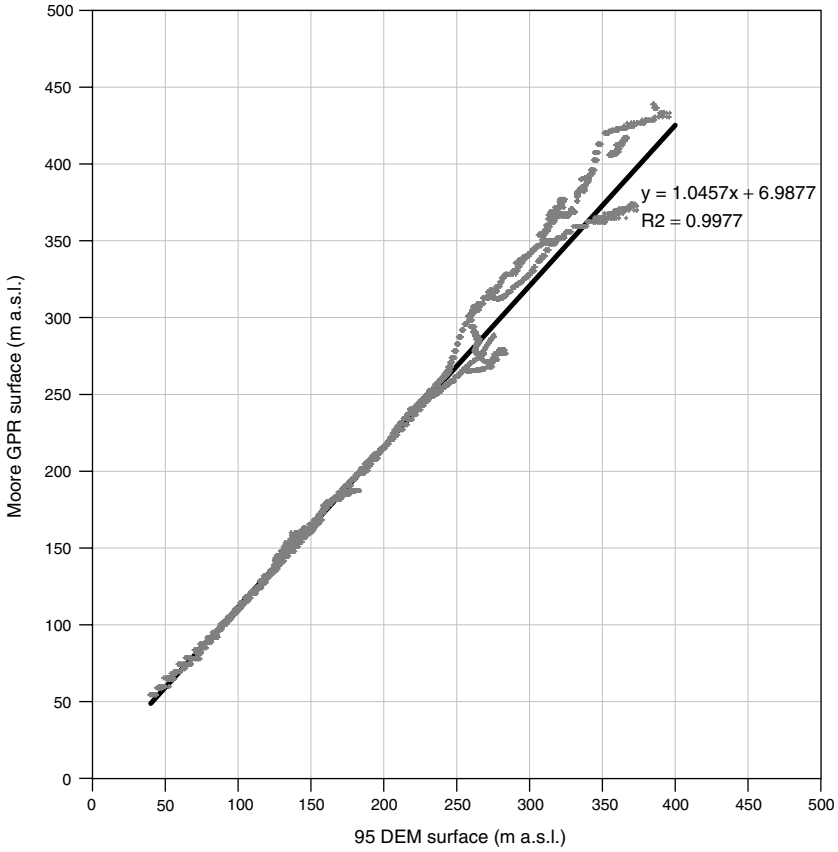

Figure 4. Regression of the 1995 GPS-derived glacier surface on the 1995 DEM surface, showing regression fitted to all points below 240 m a.s.l., extrapolated to fit all data

(v. 8·3·1). Gridded output data were transferred to the Golden Software package SURFER (v. 7·0), where boundary files were used to 'mask' the interpolated data beyond the glacier limits. Two glacier boundary files were defined. The first was derived from the 1979 Norsk Polarinstitutt 1 : 20 000 map of *Brøggerbreane, Vestre og Midre Lovénbreen*, and was used as the boundary for the surface DEM created from the same map. The second was derived, where possible, from the 1995 photogrammetrically derived data. This boundary could not be defined in some locations due to shadow, in which case the old boundary was used instead. Such a procedure means that the glacier area may have been slightly overestimated in 1995.

Theoretical drainage reconstruction

Glacier-wide subglacial drainage networks can theoretically be reconstructed from surface and bed elevation data (Shreve, 1972; Björnsson, 1982, 1988; Sharp *et al*., 1993; Flowers and Clarke, 1999; Copland and Sharp, 2000; Hagen *et al*., 2000). To illustrate the sorts of networks that may exist under Midre Lovénbreen, three steady-state subglacial water pressure conditions were assumed.

1. Water pressure (P_w) equals ice overburden pressure (P_i). P_w in a subglacial drainage network may exist at P_i (Shreve, 1972). This condition is likely where subglacial drainage elements are completely water-filled. In this case, the orientation of the drainage elements will be at right angles to hydraulic equipotential contours at the bed, from regions of higher to lower potential.
2. $P_w = 0{\cdot}5P_i$. Flowers and Clarke (1999) and Hagen *et al*. (2000) suggest that P_w may equal P_i under a glacier in winter when a hydraulically inefficient drainage system exists, but in summer P_w may drop below P_i as a consequence of surface meltwater input and the enlargement of drainage elements.

3. P_w = atmospheric pressure (P_a). Hooke (1984) suggested that if the ice is thin, the bed is steep and discharge is high, melting will exceed closure and subglacial drainage elements may exist at atmospheric pressure. If drainage elements are not completely full of water then water flow and the orientation of elements may be controlled solely by the underlying bed topography (Sharp *et al.*, 1993; Hagen *et al.*, 2000).

To reconstruct theoretically the subglacial drainage pattern, gridded values of surface and bedrock elevation were used to calculate the subglacial hydraulic potential for each of the three assumptions about subglacial water pressure discussed above. Total hydraulic potential (Φ) is the sum of the elevation and pressure potentials and can be expressed as follows (adapted from Shreve, 1972; Björnsson, 1982):

$$\Phi = \rho_w g B + C[\rho_i g(H - B)]$$

where ρ_w is the density of water (1000 kg m^{-3}), ρ_i is the density of ice (917 kg m^{-3}), g is the acceleration due to gravity (9·81 m s^{-2}), H and B are the elevations of the ice surface and subglacial topography respectively (m), and C is a constant equal to 1, 0·5 or 0 for the cases where $P_w = P_i$, $P_w = 0{\cdot}5P_i$ or $P_w = P_a$ respectively.

The upstream area across each of the hydraulic potential surfaces was mapped in order to reconstruct theoretically the overall configuration of the subglacial drainage network (Sharp *et al.*, 1993). Area is used as a surrogate for the volume of runoff generated within each grid cell. Each grid cell is assigned a 'weight' defined as its own area plus that of all upstream cells which contribute runoff to it, and each grid cell passes its weight to any adjacent cell with a lower hydraulic potential or elevation. Thus, the total area of the glacier bed contributing runoff to each grid cell is calculated. The resultant upstream area map acts as a guide to the likely location of preferential drainage axes (Sharp *et al.*, 1993). The drainage axes derived from these reconstructions will be discussed in the following section.

RESULTS

Bed DEM

The subglacial topography DEM derived from the combined data-sets is shown in Figure 5. The dominant feature is a deeply incised valley that lies beneath the centreline of the upper glacier but trends slightly west of the glacier centreline beneath the lower glacier. Towards the glacier snout this valley opens out into a plain of flatter topography.

Surface DEMs

The two surface DEMs from 1977 and 1995 are shown in Figure 6. In both years, the glacier surface is classically concave in the accumulation zone and convex in the ablation zone. At the snout, the surface slopes away to its east and west margins to form a piedmont-type lobe. This is a function of lateral spreading as the glacier exits the valley that constrains it for most of its length.

The mean annual change in height between the two surface DEMs is shown in Figure 7. Surface elevation changes are converted to metres of water equivalent (m w.e.) by multiplying by the density of ice across the whole glacier, since above the equilibrium line, snow/firn density profiles are usually consistent from year to year and surface changes should be thought of as an addition/subtraction of ice rather than snow/firn (Andreassen, 1999; Hubbard *et al.*, 2000). Most of the glacier showed surface lowering, although thickening occurred over small parts of the western and southern basins, large parts of the eastern basins, and the area on the glacier tongue fed by the eastern basins. There are two isolated regions of very high lowering (*c.* 3 m w.e. a^{-1}), one in the western basin and one in the southern basin. On average, the whole glacier thinned by *c.* 11·0 m w.e. over the 18 year period (with a root mean square error (r.m.s.e.) of ±12·8 m w.e averaged over the whole glacier; ±9·4 m w.e. below 240 m a.s.l.; and ±18·3 m above 240 m a.s.l.), corresponding to a mean annual lowering of *c.* 0·6 m w.e. a^{-1} (with a r.m.s.e. of ±0·7 m w.e. a^{-1} averaged over the whole glacier; ±0·5 m w.e. a^{-1} below 240 m a.s.l.; and ±1·0 m w.e. a^{-1} above 240 m a.s.l.). Within the thinning regions alone, mean lowering was *c.* 16·4 m w.e. (a mean annual rate of *c.* 0·9 m

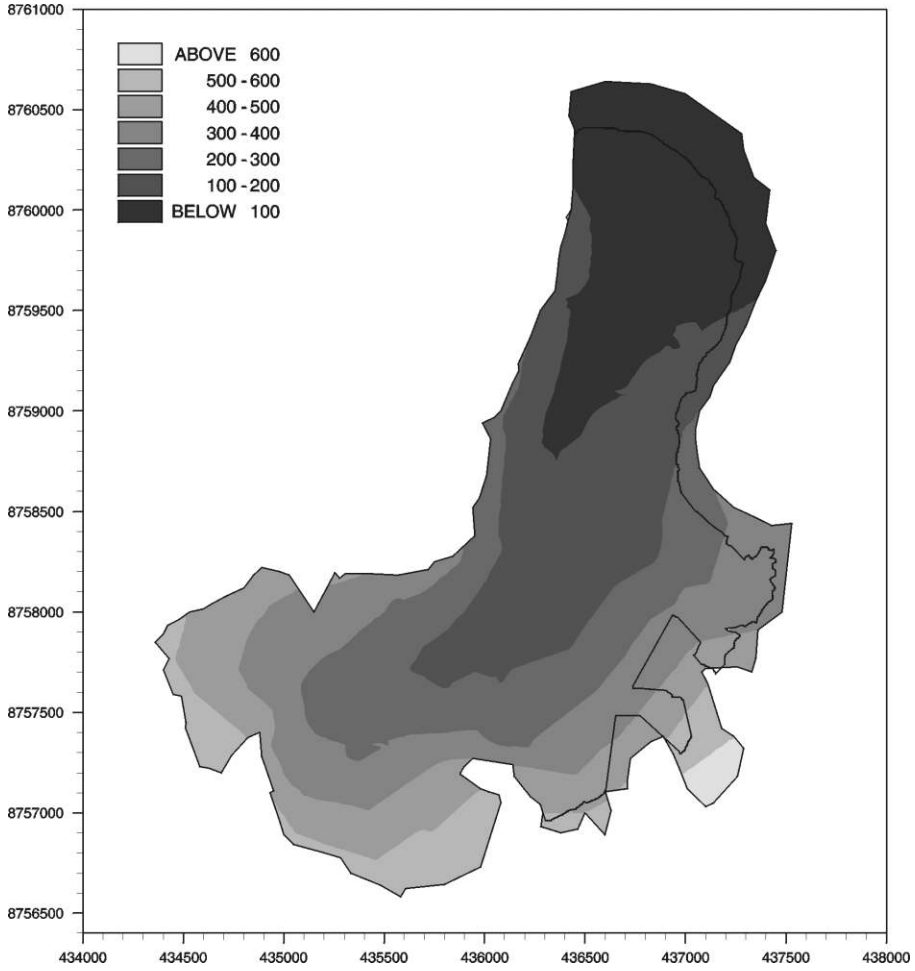

Figure 5. Subglacial topography DEMs, derived from GPR data collected by H. Björnsson in 1990 and J. Moore in 1995 (elevation in metres). The glacier is defined using the 1977 boundary, with the 1995 boundary superimposed over this. Easting on *x*-axis, northing on *y*-axis; units are metres; north is to top of figure

w.e. a^{-1}) and within the thickening regions, the mean elevation gain over the 18 year period was *c*. 15·6 m w.e. (a mean annual rate of *c*. 0·9 m w.e. a^{-1}). Clearly the errors associated with these mass balance values are very large, and these may account for all patterns of surface elevation change. Despite this, a number of possible glaciological explanations for the patterns of surface elevation change are addressed in the discussion below.

The glacier covered 5·9 km^2 in 1977 and 5·0 km^2 in 1995. This represents a loss in surface area of 0·9 km^2 over the 18 year period, equivalent to an annual rate of *c*. 0·05 km^2 a^{-1}. The glacier snout retreated by *c*. 150 m in the 18 year period, a mean rate of *c*. 8·3 m a^{-1}. The eastern margin of the tongue also retreated at a mean rate of *c*. 5·6 m a^{-1}. Elsewhere, specifically to the west and the southwest, little or no change in the boundary could be discerned, although this was due partly to limitations in boundary definition from the 1995 air photos. In 1977 the volume of the glacier was $3{\cdot}9 \times 10^8$ m^3 (with a maximum error (assuming 15 m error in the bed, and 10 m error in the surface) of $\pm 1{\cdot}5 \times 10^8$ m^3). In 1995 the volume had decreased to $3{\cdot}2 \times 10^8$ m^3 (with a maximum error of $\pm 1{\cdot}2 \times 10^8$ m^3). This represents a decrease of $7{\cdot}1 \times 10^7$ m^3 ($6{\cdot}5 \times 10^7$ m^3 w.e.), or *c*. 18·3 per cent by volume. However, the errors associated with this volume change are large at $1{\cdot}9 \times 10^8$ m^3 ($1{\cdot}8 \times 10^8$ m^3 w.e.). On an annual basis, this represents a volume loss of $3{\cdot}9 \times 10^6$ m^3 a^{-1} ($3{\cdot}6 \times 10^6$ m^3 w.e. a^{-1}), with associated errors of $1{\cdot}1 \times 10^7$ m^3 ($9{\cdot}7 \times 10^6$ m^3 w.e.).

With maximum errors, these volume changes are not significant. Notwithstanding these errors, the possible significance of such changes for glacier mass balance is addressed in the discussion section below.

Equipotential contours

Contours of hydraulic equipotential assuming $P_w = P_i$ and $P_w = 0{\cdot}5P_i$ in 1977 and 1995 are shown in Figure 8. Contours of equipotential for $P_w = P_a$ are exactly the same as bed contours which are shown in Figure 5. There is a maximum possible error of ± 15 m in the bed DEM and a maximum possible error of ± 10 m in the surface DEM. Together this means that the ice thickness may be overestimated or underestimated by a maximum of 25 m. Any error in the surface and/or bed DEM is likely to be systematic rather than random, and so to test the effects of this systematic error, equipotential contours were reconstructed assuming the thickest possible glacier and the thinnest possible glacier, for all possible pressure scenarios. In all cases, there was no discernible difference between these reconstructions, and those presented in Figure 8.

Hydraulic equipotential contours, when $P_w = P_i$, bear a close resemblance to contours of surface elevation (cf. Figure 6). There is little difference between the two plots for $P_w = P_i$ in 1977 and 1995, apart from changes associated with the different boundary. When $P_w = 0{\cdot}5P_i$, bed topography has a bigger influence on hydraulic potential than it does when $P_w = P_i$ and the contours of equipotential more closely resemble those of the bed (cf. Figure 5).

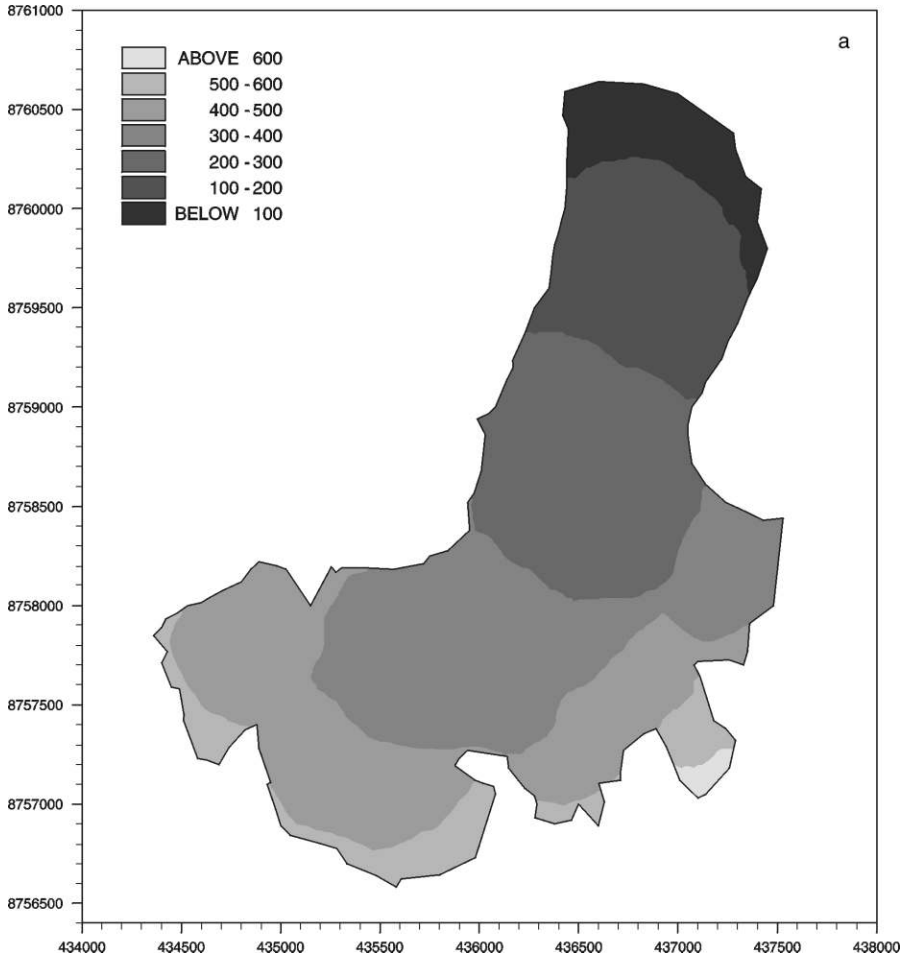

Figure 6. Surface DEMs from (a) 1977 and (b) 1995 (tuned); (elevations in metres). Easting on *x*-axis; northing on *y*-axis; units are metres; north is to top of figure. Surface data reproduced with permission from The Norwegian Polar Institute ©

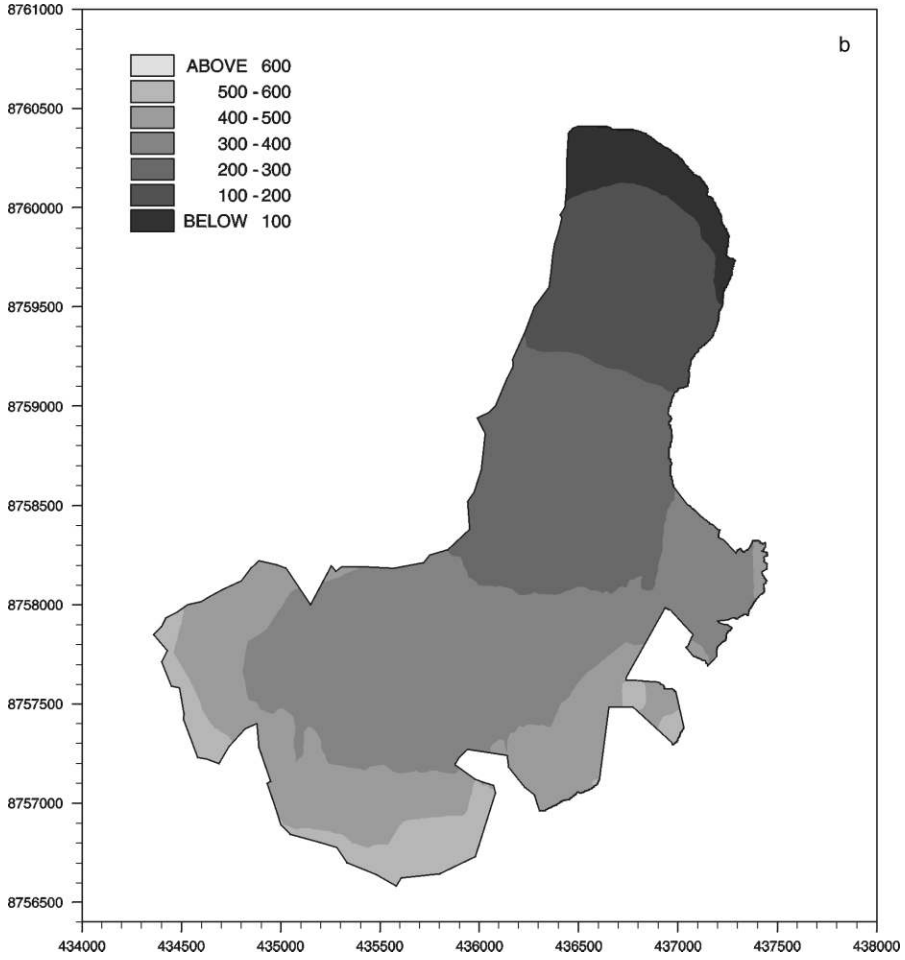

Figure 6. (*Continued*)

Theoretical drainage reconstruction

The three possible theoretical drainage reconstructions for 1977 are shown in Figure 9a–c and those for 1995 are shown in Figure 9d–f. The maximum possible systematic error in ice thickness of ±25 m was tested for its impact on theoretical drainage reconstructions as it had been on the equipotential contours. In all cases, there was again found to be no discernible difference between these reconstructions, and those presented in Figure 9. In Figure 9, higher values of upstream area in any cell indicate greater theoretical water discharge through the cell. Conversely, lower values indicate smaller theoretical discharge. As water discharge is one of the main controls on the morphology of subglacial drainage systems (Röthlisberger and Lang, 1987; Hooke, 1989; Hubbard and Nienow, 1997; Fountain and Walder, 1998), the axes of high upstream area are likely to represent routes of hydraulically efficient high discharge drainage, while zones of low upstream area probably indicate areas of hydraulically inefficient low discharge drainage. Where water in one cell is passed to several downglacier cells, theoretical discharge decreases downglacier. In such cases, we envisage that hydraulically efficient routeways meet inefficient areas, water is dispersed across a large area of the bed, and water flow may be restricted and ponding might occur. In the following discussion, we continue this theoretical assumption that high upstream area equates with hydraulically efficient high discharge drainage, and that low upstream area is synonymous with hydraulically inefficient low discharge drainage.

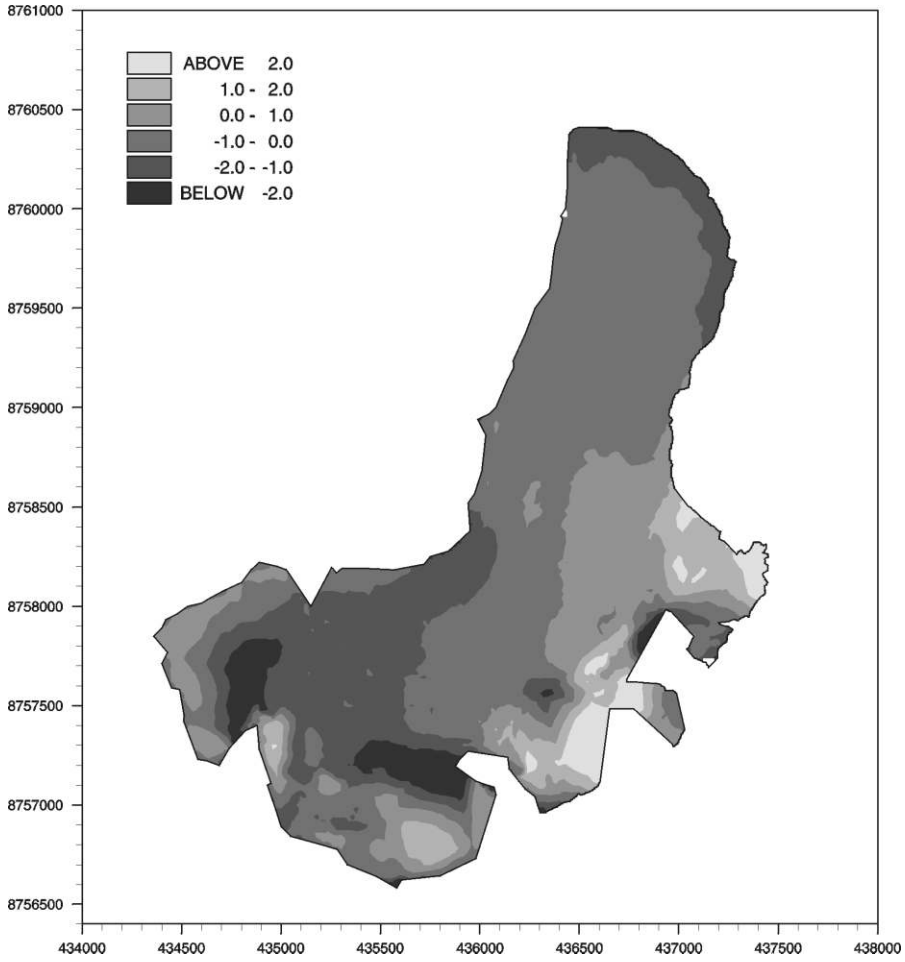

Figure 7. Surface height change (m w.e. a^{-1}) between 1977 and 1995. Negative values indicate decreasing height (thinning); positive values indicate increasing height (thickening). Easting on *x*-axis; northing on *y*-axis; units are metres; north is to top of figure

1977, $P_w = P_i$ (Figure 9a). Here, a high discharge routeway runs down the glacier to the west of the glacier centreline. Approximately 1 km from the terminus, this routeway bifurcates to form three primary branching pathways heading to the western, central and eastern parts of the snout. There is also a secondary bifurcation from the eastern arm that also reaches the snout. Because of the likely high discharges involved, water routing in these pathways is probably relatively hydraulically efficient.

1977, $P_w = 0{\cdot}5P_i$ (Figure 9b). The central high discharge routeway has been lost, and only a few isolated patches of equivalent high discharge exist. The routeway is discontinuous, with major breaks, most noticeably towards the snout. At the snout, the three branching pathways can still be seen and there is an additional pathway to the eastern margin. However, these branches are not joined to the high discharge routeway beneath the tongue, as they were when $P_w = P_i$. Only the pathway flowing beneath the eastern part of the snout, carrying the majority of subglacial drainage water to the terminus, appears to be fed by the main routeway, but even this is detached from it by an area of less hydraulically efficient drainage. Overall, drainage is likely to be less efficient than the case when $P_w = P_i$ because discharge is less and the pathway must negotiate low-discharge areas.

1977, $P_w = P_a$ (Figure 9c). This model bears some resemblance to that when $P_w = 0{\cdot}5P_i$, with small isolated areas of high discharge in the upper glacier. The main drainage routeway carries water at similar discharge to that when $P_w = 0{\cdot}5P_i$; however, it is even more discontinuous, most noticeably towards the

snout. These features are regions of very shallow bed gradients where weight is passed to all downstream cells. Drainage is likely to be dispersed in these regions which possibly represent areas of water ponding. Water is likely to be routed inefficiently to the snout. There is only one outlet at the terminus in the centre of the snout in the deepest part of the bedrock valley.

1995, $P_w = P_i$ (Figure 9d). Here, there is a wide high discharge drainage routeway, to the west of the centreline, with moderately high discharges across most of the tongue, similar to the pattern in 1977. There are three main changes since 1977. First, the moderate discharge areas in the western accumulation basin do not feed directly into the high discharge routeway beneath the tongue but are connected instead via lower discharge areas. This change is a consequence of changing ice surface slope. In 1977, steeper surface slopes were able to direct water efficiently over the shallow bed slopes but in 1995, when surface slopes were gentler, drainage was less efficient across the bed and water may have been temporarily ponded. Second, the high discharge routeway in the middle-to-upper part of the glacier tongue braids around a region of lower discharge. This is also a consequence of a reduction in ice surface slope. Third, within the snout region drainage still occurs to the west, but the two main outlets to the central and eastern parts of the terminus are reduced to a single outlet between the two.

1995, $P_w = 0{\cdot}5P_i$ (Figure 9e). The drainage pattern is very similar to that in 1977. Isolated patches of high discharge exist in the upper and central glacier. As in 1977 there are major breaks in this routeway close to the snout. Once again, there are a number of locations where primary pathways reach the terminus but the dominant one seems to flow to the east. One major change since 1977 seems to be that a pathway no longer reaches the western part of the snout.

1995, $P_w = P_a$ (Figure 9f). The drainage pattern is virtually identical to that in 1977. This is expected since apart from the effects of boundary changes, subglacial topography (on which this reconstruction is based) is unchanged between 1977 and 1995. However, because of the change in snout position, there is no equivalent proglacial outlet in the centre of the snout, as seen in 1977. Instead, a small isolated region of moderate discharge can be seen in the eastern part of the snout, but this is separated from upglacier drainage of similar discharge by a large region of dispersed inefficient drainage.

DISCUSSION

Changes in glacier geometry

The glacier shrank from 5·9 km^2 in 1977 to 5·0 km^2 in 1995 representing an average loss of *c*. 0·05 km^2 a^{-1}. The glacier snout retreated by *c*. 150 m in the 18 year period at a mean rate of *c*. 8·3 m a^{-1}. The glacier volume was $3{\cdot}9 \times 10^8$ m^3 in 1977 but only $3{\cdot}2 \times 10^8$ m^3 in 1995, representing a decrease of $7{\cdot}1 \times 10^7$ m^3 ($6{\cdot}5 \times 10^7$ m^3 w.e.), or *c*. 18 per cent by volume. On an annual basis, this represents a volume loss of $3{\cdot}9 \times 10^6$ m^3 a^{-1} ($3{\cdot}6 \times 10^6$ m^3 w.e. a^{-1}). However, the errors associated with this apparent loss are large: $1{\cdot}1 \times 10^7$ m^3 ($9{\cdot}7 \times 10^6$ m^3 w.e.).

Although errors may be responsible for all the apparent changes in glacier elevation, particularly above 240 m a.s.l., a number of glaciological explanations may also be responsible. Our results suggest that enhanced thinning occurred in two main areas in the western and southern accumulation basins (Figure 7). These areas are coincident with zones of higher surface slope and exposed ice, containing small crevasses visible in the 1995 air photographs. It seems likely that these locations are swept clear of snow by wind scour and sloughing so that there is no net accumulation here. In addition, these areas might experience high ablation due to high net short-wave radiation receipts because the ice has a lower albedo than that of snow, and because the crevasses expose a greater surface area to ablation (Pfeffer and Bretherton, 1987). Furthermore, because these regions are steep, ice flow may be faster than the surrounding ice, and so enhanced thinning here may be due to high rates of longitudinal extension and vertical compression in these areas.

Thickening occurred in all the accumulation basins towards the rock-walls (Figure 7). Net accumulation might be expected in these regions for three reasons. First, wind-carried snow might drift against the surrounding slopes. Second, sloughing and avalanching might occur off the steep slopes. Third, incoming short-wave radiation might be reduced due to the effects of shading in these basins. Areas of enhanced

thickening (*c*. 2–3 m w.e. a^{-1}) are found in the eastern basins (Figure 7). Enhanced thickening here may be a consequence of these three factors acting to a greater degree.

Thickening also occurred in the upper eastern tongue at a rate of *c*. 0–1 m w.e. a^{-1}. This thickening may be due to persistently more compressive horizontal ice flow here, compared with surrounding areas, as a result of faster moving ice from the steeper eastern basins meeting slower moving ice on the glacier tongue. Horizontal compression may be particularly marked here because this part of the tongue is cold-based but the eastern basins may be warm-based as a consequence of the insulating effects of the winter snow cover, and the release of latent heat by refreezing meltwater in the firn during the summer (Björnsson *et al*., 1996).

The overall reduction in glacier area and volume is in accordance with the retreat and thinning that has been documented for most valley-glaciers worldwide over the last 40 years (Dyurgerov and Meier, 1997). Assuming a constant rate of retreat, the calculated rate of retreat of the snout of *c*. 8·3 m a^{-1} is in good agreement with suggestions that Midre Lovénbreen has receded almost 1000 m since the Neoglacial Maximum in *c*. 1890 (Hansen, 1999, in Glasser and Hambrey, 2001). However, the mean annual balance of −0·61 m w.e. a^{-1} calculated here indicates greater mass loss than that derived from the Norsk Polarinstitutt mass balance data, for 1977–1995, of −0·35 m w.e. a^{-1} (Hagen and Liestøl, 1990; IAHS/UNEP/UNESCO, 1993; IAHS/UNESCO, 1998; Lefauconnier *et al*., 1999). Thus the field-measured value is only *c*. 57 per cent of our value determined from sequential DEMs. However, our errors associated with mass balance changes are large

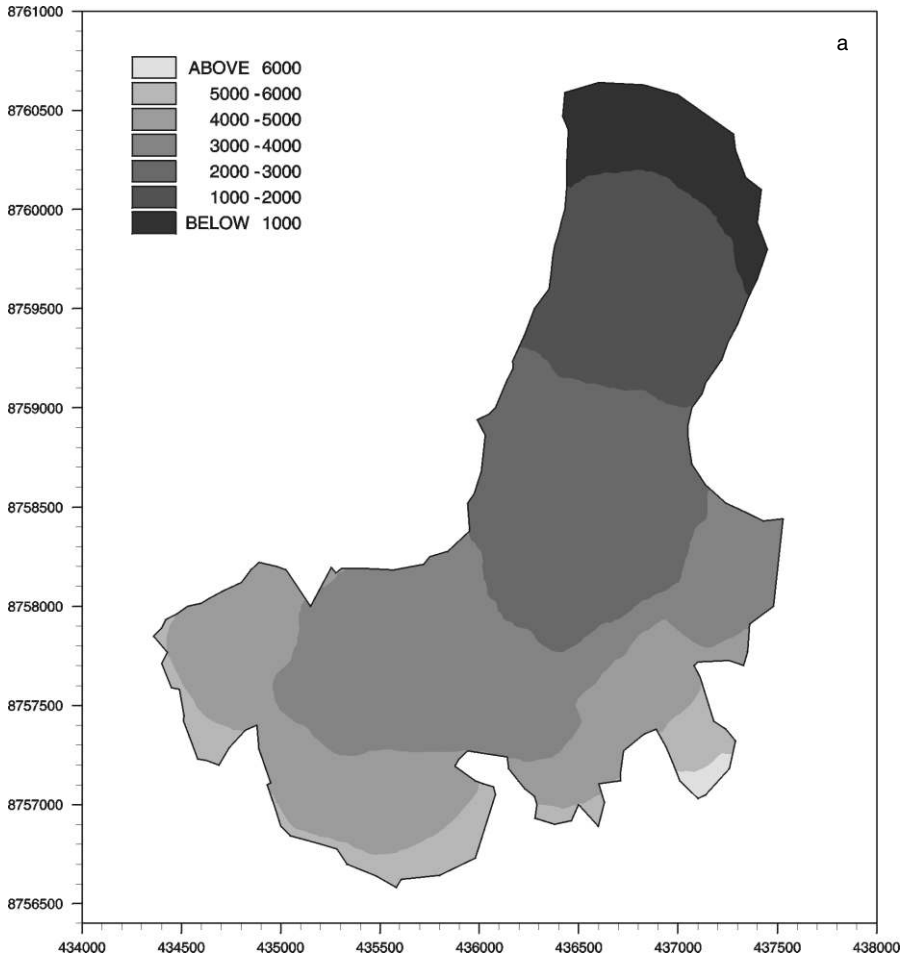

Figure 8. Contours of hydraulic equipotential (in kPa): (a) $P_w = P_i$ in 1977; (b) $P_w = 0{\cdot}5P_i$ in 1977; (c) $P_w = P_i$ in 1995; (d) $P_w = 0{\cdot}5P_i$ in 1995. Easting on *x*-axis; northing on *y*-axis; units are metres; north is to top of figure

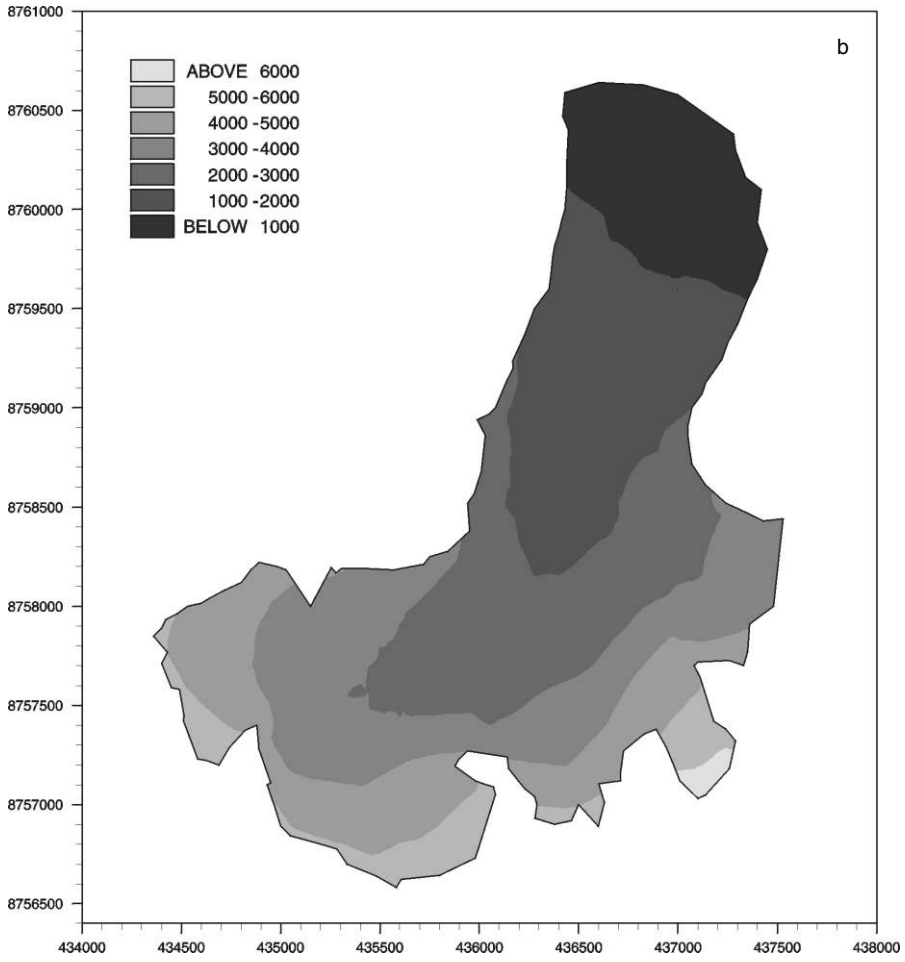

Figure 8. (*Continued*)

and may explain all apparent discrepancies with the field-based measurements. Despite this, similar findings were also reported recently for Finsterwalderbreen in southwest Spitsbergen where the mean annual balance between 1970 and 1990 calculated from sequential DEMs was $-0{\cdot}65$ m w.e. a^{-1} but that measured in the field between 1950 and 1995 was only *c*. $0{\cdot}45$ m w.e. a^{-1} (Hagen *et al*., 2000). Thus, the field measured value was only *c*. 69 per cent of the sequential DEM-determined value. Furthermore, a recent energy balance model was used to calculate the mean annual balance of Midre Lovénbreen between 1980 and 1989 (Fleming *et al*., 1997). It calculated a mean annual balance of $-0{\cdot}44$ m w.e. a^{-1} compared with a measured mean annual balance over the same period of $-0{\cdot}27$ m w.e. a^{-1}. This represents a field-measured value which is only *c*. 61 per cent of the modelled one. From our evidence and that of Hagen *et al*. (2000) and Fleming *et al*. (1997) it appears that the field measurements of mass balance on Midre Lovénbreen (and possibly other Svalbard glaciers) may be underestimating the real mass balance. This implies that the ablation and accumulation measurements made at stakes and in pits along the glacier centreline might be underestimating the ablation and/or overestimating the accumulation for equivalent altitudes across the glacier. This may be explained if: (i) net ablation in the ablation zone is higher towards the glacier margins than at the centreline due to the influence of long-wave radiation or advection of turbulent energy from the valley sides; and/or (ii) net accumulation in the accumulation zone is lower towards the glacier margins than at the centreline due to the effects of the valley sides on both winter accumulation and summer ablation.

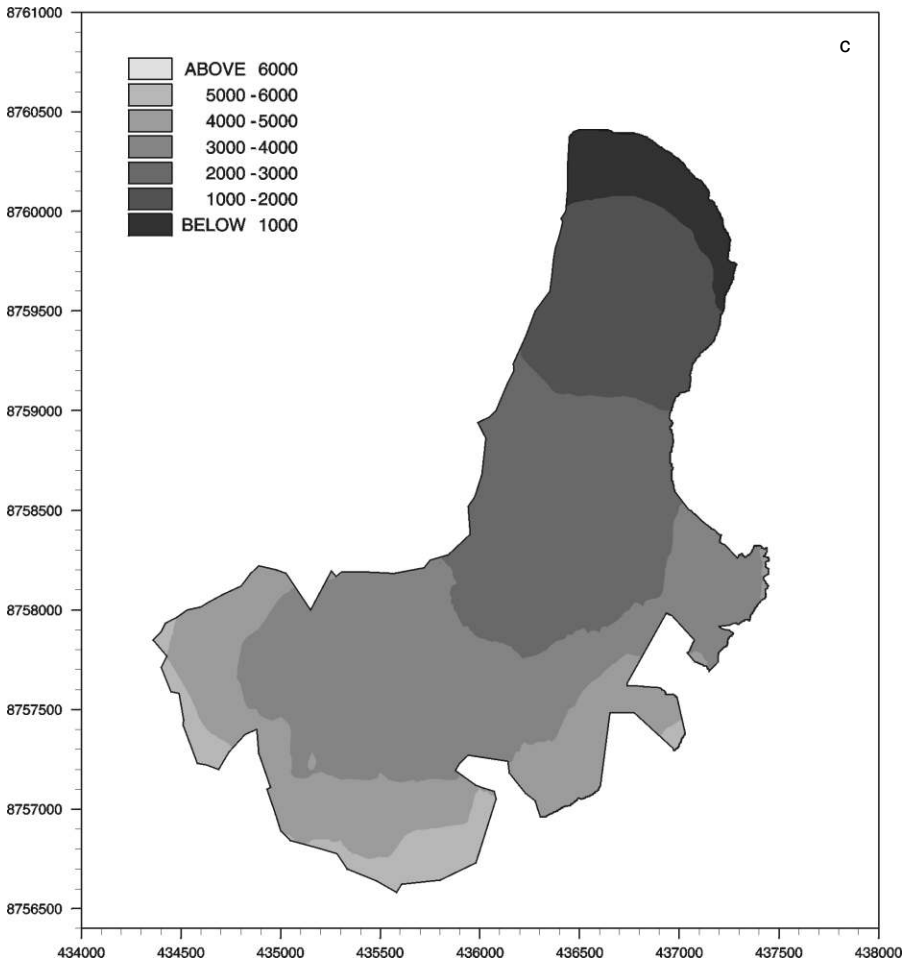

Figure 8. (*Continued*)

Theoretical drainage patterns under different pressure regimes

The three assumptions about subglacial water pressure, $P_w = P_i$, $P_w = 0{\cdot}5P_i$ and $P_w = P_a$, lie on a continuum. Decreasing water pressure leads to a relative decrease in the influence of surface morphology and a corresponding increase in the effects of bed topography. In both 1977 and 1995 under all three scenarios, the main preferential drainage axis flows close to the centreline beneath the upper glacier and slightly to the west of the centreline beneath the lower glacier (Figure 9). In both 1977 and 1995 there are four main effects of decreasing water pressure (Figure 9).

First, beneath the glacier tongue, high discharge drainage routeways become narrower, more tortuous and more broken, and more of the bed is drained at lower discharges. Thus, decreasing water pressure is likely to be associated with more dispersed, less hydraulically efficient drainage. The same conclusion was reached for similar studies undertaken on Haut Glacier d'Arolla, Switzerland (Sharp *et al*., 1993) and Trapridge Glacier, Yukon Territory (Flowers and Clarke, 1999). It appears that the relatively gentle bed gradients of these glaciers make them predisposed to dispersed drainage at low water pressures but the relatively steep surface slopes make concentrated drainage more probable at high water pressures. Second, towards the top of the glacier, the high discharge routeway migrates from the southern basin towards the western basin and the drainage system beneath the western basin becomes increasingly connected to the main drainage routeway running down the glacier tongue. This latter point is contrary to that discussed in point one above and is a consequence of the

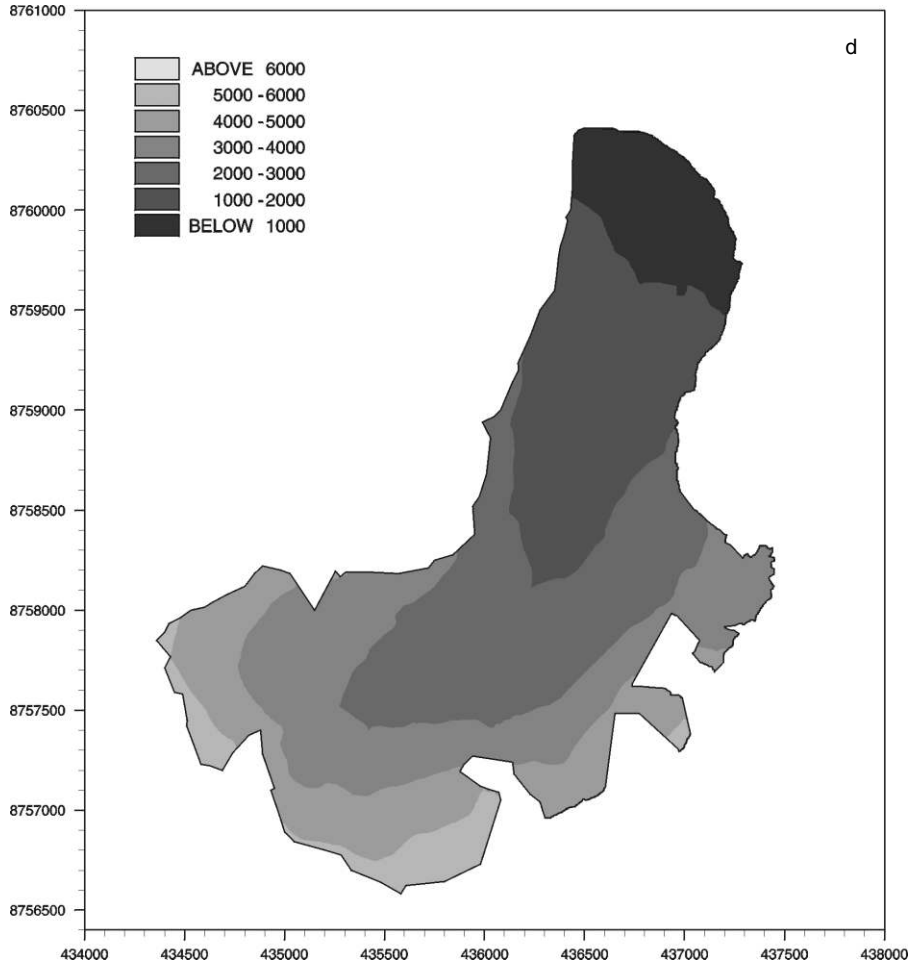

Figure 8. (*Continued*)

relatively shallow surface slopes and steep bed slopes in this region. Thus, at high water pressures shallow surface slopes in the western basin mean flow is inhibited and ponding may develop. As pressures drop, this becomes less likely as the steep bed slopes exert more influence on drainage. Third, near the glacier snout there is a reduction in the number of branching pathways that are connected to the main drainage routeway beneath the tongue. Pathways become increasingly susceptible to the effects of shallow bed slopes, which prevent water from easily exiting the glacier, and possibly lead to regions of ponding. Fourth, also near the glacier snout, water is increasingly routed away from the western half of the terminus towards the eastern half.

Changes in subglacial drainage at the snout between 1977 and 1995

Some of the biggest changes in surface topography between 1977 and 1995 occurred towards the glacier snout and these have had important effects on the theoretical pattern of subglacial drainage beneath this region. The suggested changes are different depending on assumptions about the water pressure regime. Thus, if water pressures are high, it seems likely that high discharge outflow would have become increasingly directed towards the western half of the snout (Figure 9a and d). However, for moderate water pressures it appears as though moderate discharge outflow would have become increasingly routed to the central and eastern parts of the snout (Figure 9b and e). For water pressures equal to atmospheric, hydraulically inefficient

drainage would be expected to emerge from the central part of the snout in 1977, while in 1995, inefficient drainage would emerge to the east (Figure 9c and f).

Theoretical and observed subglacial drainage at the snout

To identify which of our assumptions about the water pressure regime is likely to be most accurate, we compare the theoretical drainage reconstructions for 1995 (Figure 9d–f) with observations of subglacial drainage outlets made by at least one of the authors during the summers of 1992, 1994, 1996, 1997, 1998, 1999 and 2000. Subglacial outlets were identified on the basis of water quality, which is good evidence of subglacial routing of meltwater (Stone and Clarke, 1996; Tranter *et al*., 1996; Wadham *et al*., 1998, 2000; Skidmore and Sharp, 1999; Hodson *et al*., 2000). In 1992, 1994, 1996, 1997 and 2000, water emerged in a single subglacial outlet in the form of a proglacial pressurized upwelling towards the eastern part of the glacier snout. In 1999, drainage was initially from the central part of the snout but then switched to an upwelling towards the east. The location of the eastern upwellings varied slightly between each year, and the eastern proglacial region is peppered with signs of many different upwelling locations. In 1998, however, there was no eastern upwelling and water exited in just one subglacial outlet towards the western part of the snout.

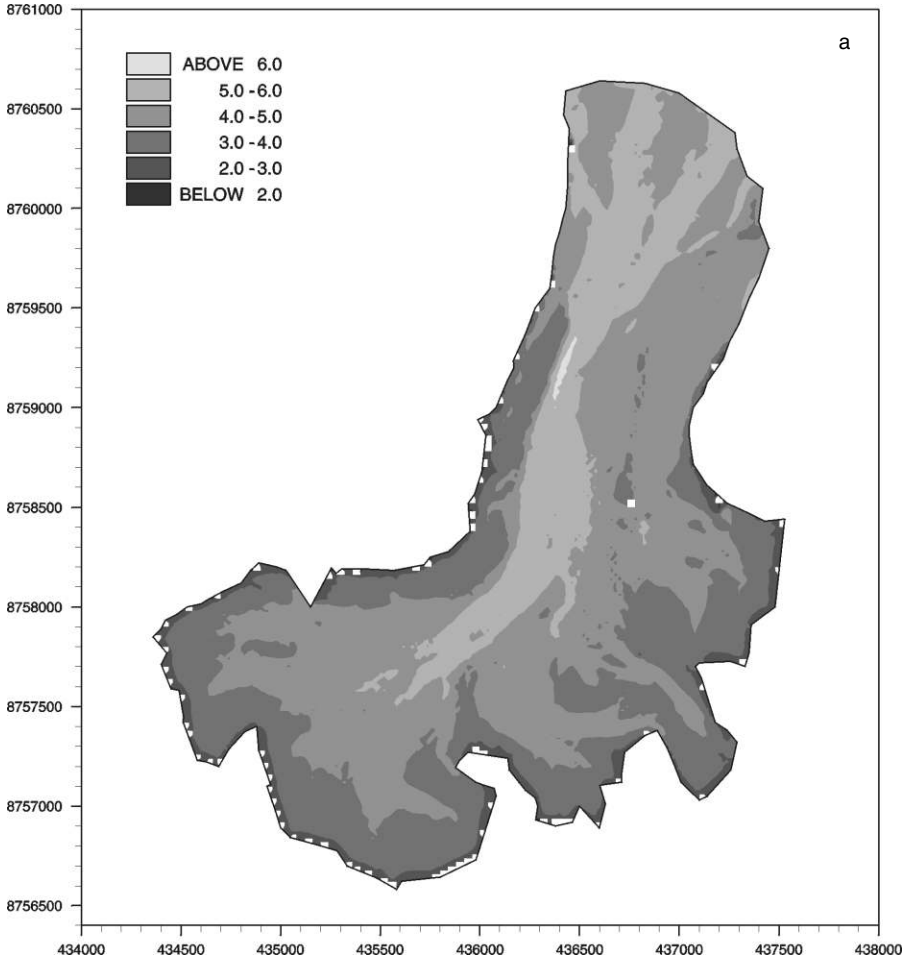

Figure 9. Upstream area plots in 1977 and 1995, based on weight passed to all adjacent cells with lower potential: (a) 1977, $P_w = P_i$; (b) 1977, $P_w = 0{\cdot}5P_i$; (c) 1977, $P_w = P_a$; (d) 1995, $P_w = P_i$; (e) 1995, $P_w = 0{\cdot}5P_i$; (f) 1995, $P_w = P_a$. Plotting logarithms of upstream area (in m^2) removes the inevitable downslope trend in area increase which hides other detail (Sharp *et al*., 1993; Flowers and Clarke, 1999). Isolated white grid-cells indicate no upstream contributing area. Easting on *x*-axis; northing on *y*-axis; units are metres; north is to top of figure

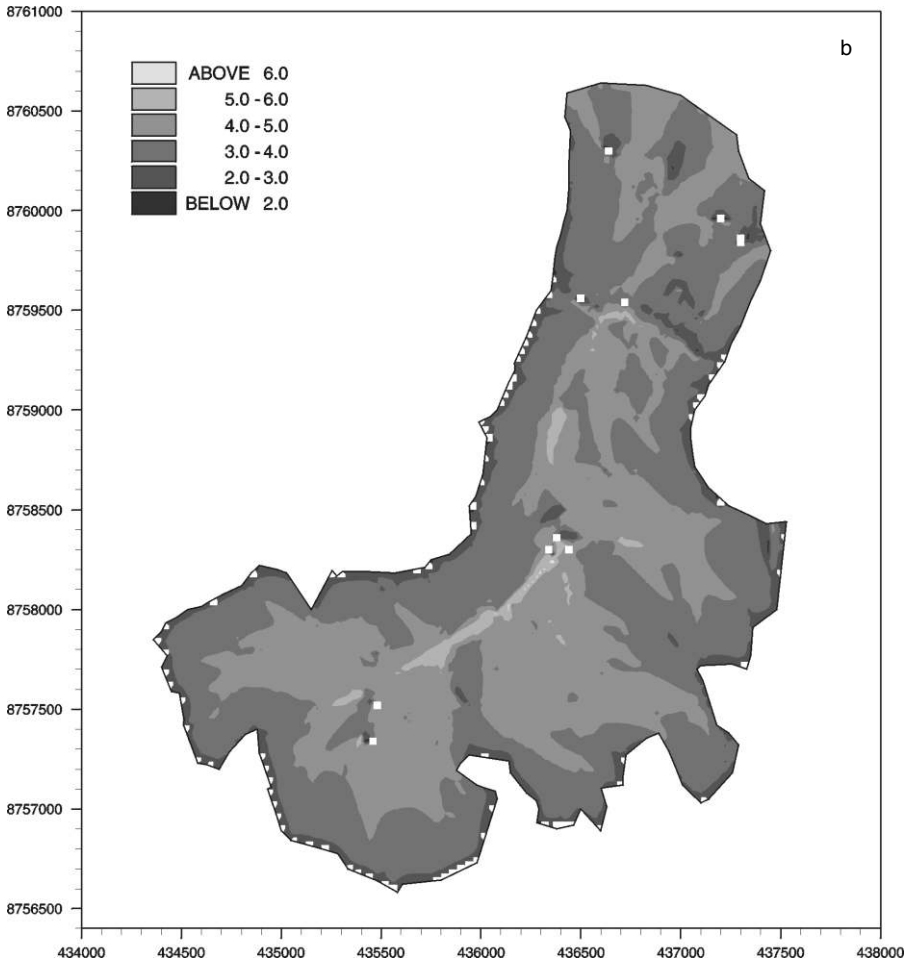

Figure 9. (*Continued*)

This outlet emerged at the glacier margin through a large, pre-existing oversized tunnel, *c*. 2 m in diameter, but originated from *c*. 8 m within the glacier where the tunnel was almost circular and <1 m in diameter. At this point, the water was almost certainly pressurized as water temperatures were negative. It is thought that a significant but temporary reorganization of the subglacial drainage system occurred in 1998, and that this was responsible for the switch in the outlet location (Hodson *et al*., 2000).

Comparing these observations with our 1995 theoretical drainage reconstructions (Figure 9d–f) suggests that in most years, steady-state water pressures are about half ice overburden at the time when drainage is established and water is preferentially routed towards the eastern snout region. Observations in 1998 imply that steady-state water pressures may have been approaching ice overburden when drainage was established in this year, directing subglacial waters to the western snout region. Drainage reconstructions for 1977 (Figure 9a–c) support the suggestion that a pre-existing channel was reoccupied in 1998. These show that drainage towards the western part of the snout was more likely in previous years (for both $P_w = P_i$ and $P_w = 0{\cdot}5P_i$). A *c*. 1–2 m diameter channel is likely to survive several years in the terminus region of Midre Lovénbreen as the creep rate of cold, thin ice is very low.

To see whether higher subglacial water pressures at the start of the melt season were more likely in 1998 than in the other years for which we have subglacial drainage outlet observations, we examined the meteorological data collected at Ny-Ålesund, *c*. 4·5 km to the northwest of Midre Lovénbreen. Unfortunately,

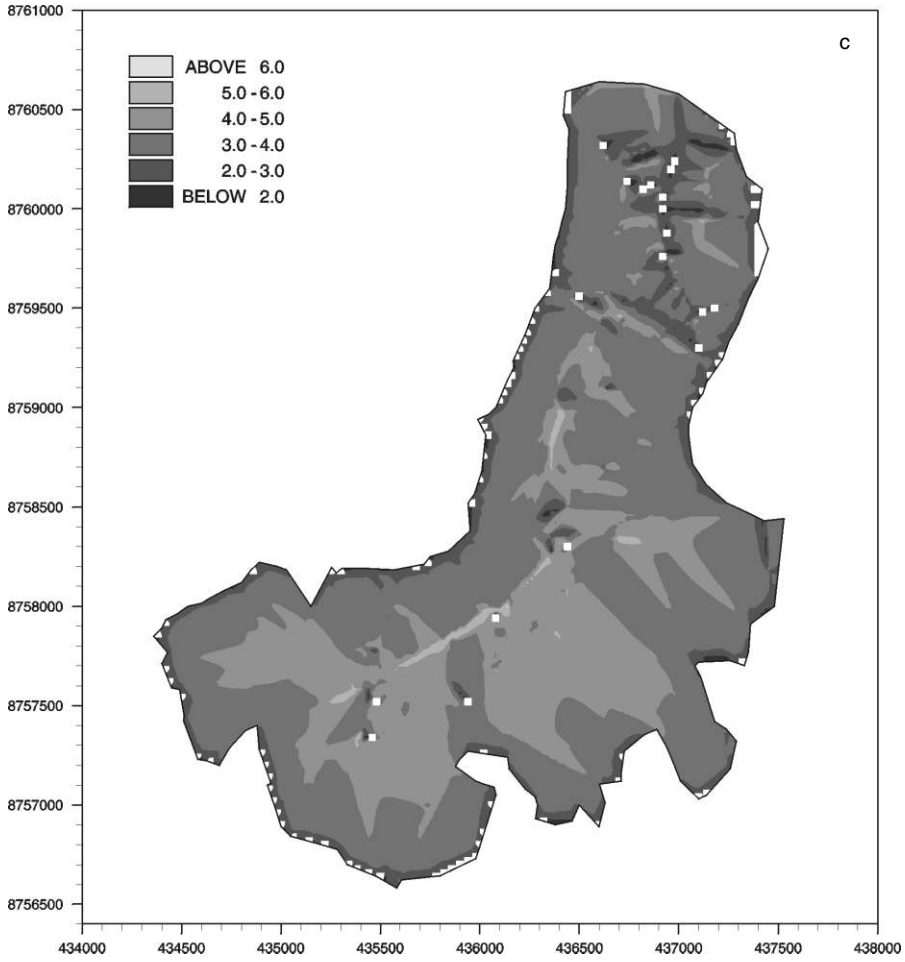

Figure 9. (*Continued*)

snow depth data are not recorded at this weather station and so we used the precipitation and air temperature data to drive a snow accumulation and ablation model (Kohler, unpublished data). The model accumulates snow when precipitation occurs and temperatures are less than 0 °C. Ablation is modelled using a degree-day approach with different degree-day factors depending on snowpack age. Model outputs show that 1998 was, indeed, anomalous. First, in 1998 snow continued to accumulate until maximum snow depths of nearly 4 m w.e. were reached in mid-May. In all other years, maximum snow depths of *c*. 2–3 m w.e. were reached in late April to early May. Second, in 1998 appreciable melting did not start until early June, whereas significant melting began in early to mid-May in the other years. Third, in 1998 rainstorms were infrequent during May and June but were much more common in the other years. Finally, in 1998 the rate of change of melting was particularly marked during early July, being greater than that occurring at any time in other years. This suggests that when moderate melting and/or rainfall occurs in late spring, water is able to gradually enlarge subglacial drainage pathways allowing water to flow at pressures below ice overburden and be routed to the eastern snout. In 1998, when rapid melting started in early summer, water was unable to enlarge subglacial drainage pathways sufficiently, and water was routed to the western snout at pressures approximating ice overburden.

We can also compare the theoretical drainage reconstructions for 1995 (Figure 9d–f) with observations of the position of a proglacial icing (also known as naled or aufeis). Icings are common features of polythermal

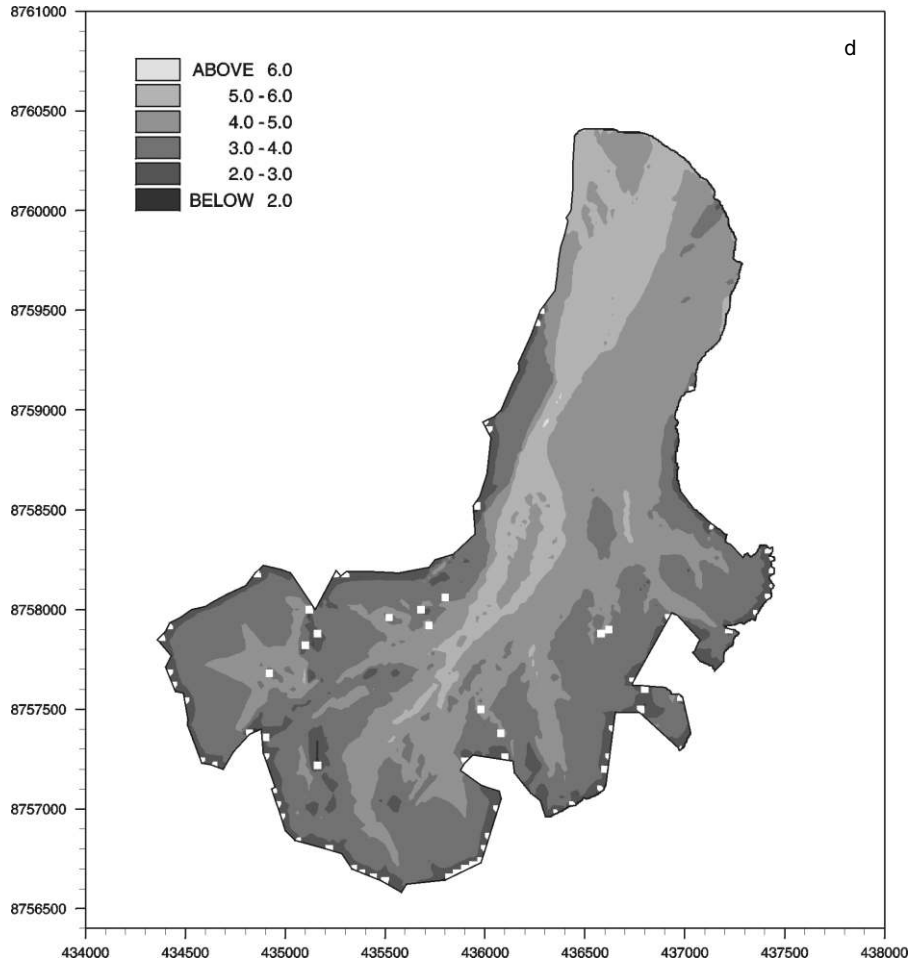

Figure 9. (*Continued*)

glaciers; they form proglacially during the winter by the refreezing of water from a variety of sources, including a proportion which is subglacially derived, and they indicate water flow through permeable sediments beneath a permafrost layer (Liestøl, 1977; Hodgkins, 1994; Wadham *et al*., 2000). At Midre Lovénbreen, an icing forms *c*. 250 m from the central part of the glacier snout. Icings do not form in the eastern or western parts of the proglacial area where, as has been discussed, subglacial drainage is most likely to emerge. The 1995 drainage reconstructions when $P_w = P_i$ and $P_w = 0{\cdot}5P_i$ (Figure 9d and e) both have potential to route water to the central snout. Because the central routeway, rather than the eastern or western outlet, is used during the winter, other factors, such as sediment thickness or permeability and permafrost depth, must inhibit water flow to the east and west.

Mechanisms of subglacial drainage beneath the snout

Water may access warm-based ice at the bed of Midre Lovénbreen via temperate accumulation areas and via deeply incised supraglacial channels which are reused year after year, and cut down through the cold surface layer (Liestøl *et al*., 1980; Hagen *et al*., 1991; Björnsson *et al*., 1996). Assuming water is able to access the bed in this way, the location of the major theoretically reconstructed drainage axes may be realistic where they coincide with the location of basal temperate ice. However, beneath the cold snout, theory suggests there should be no drainage since cold ice should act as an aquiclude (Hodgkins, 1994, 1997). However, our drainage reconstructions for pressurized water accurately predict the location

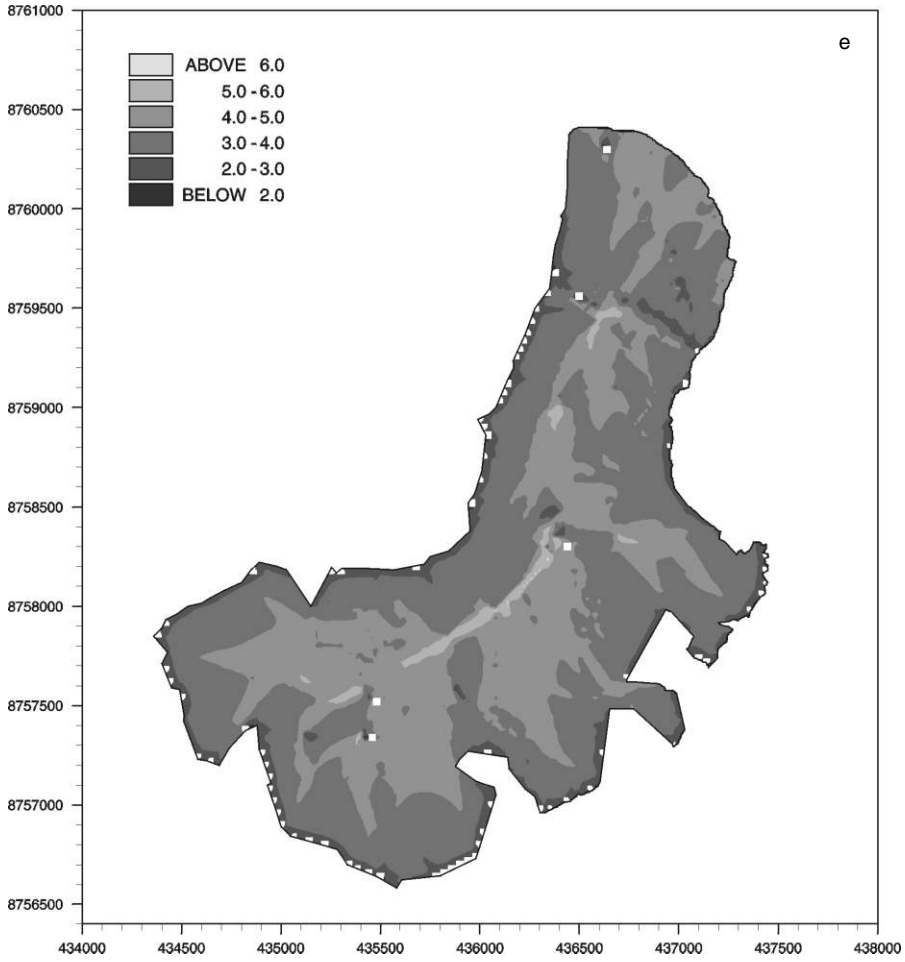

Figure 9. (*Continued*)

of major outlet streams, which suggests that equipotential contours across the bed do influence the position of preferential drainage axes, even beneath the cold-based margins. This suggests that water directed beneath warm-based ice in the central part of the glacier tongue, is able to escape through the cold-based terminus. Two possible mechanisms suggest themselves. The eastern upwelling emerges in variable locations from year to year, through proglacial sediments a few metres in front of the glacier margin. This suggests that water may flow under the permafrost beneath the cold-based glacier snout and emerge through a fissure in the proglacial sediments. Water may be forced into a sub-permafrost location at the boundary between cold and temperate ice, and once here, the orientation of drainage elements might be controlled by differences in equipotential pressure, as in a subglacial location. The same mechanism has been suggested to explain observations from Werenskiold Glacier, Finsterwalderbreen, Hessbreen, Erdmannbreen and Austre Lovénbreen, all in Svalbard (Krawczyk, 1992; Wadham *et al*., 1998; Hodson and Ferguson, 1999). Conversely, the western outlet emerges from within the glacier from a large pre-existing ice-walled conduit flowing across the glacier bed. It is not known how far this conduit extends beneath the cold-based snout, although evidence suggests that in 1998 water emerged under pressure *c*. 8 m upglacier from the terminus. Perhaps the higher water pressures beneath the warm-based ice that directed water to the west of the glacier in 1998 were sufficient to cause hydrofracturing through the basal ice and/or hydraulic jacking beneath the basal ice allowing water to escape from the pre-existing conduit. A similar mechanism was

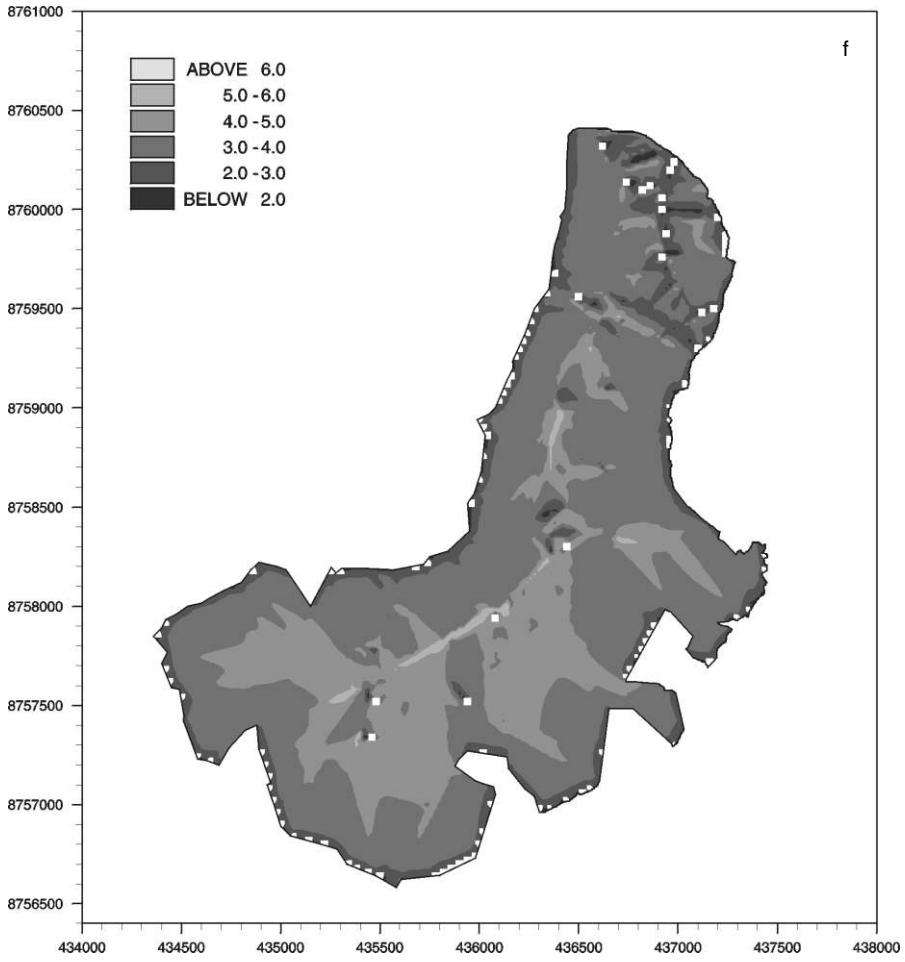

Figure 9. (*Continued*)

advanced to explain observations at the snout of John Evans Glacier, Ellesmere Island (Skidmore and Sharp, 1999).

CONCLUSIONS

We have used a bed DEM and surface DEMs to identify changes in the geometry of Midre Lovénbreen, Svalbard, between 1977 and 1995. Although spatial patterns of glacier volume change may be accounted for by errors, they may also be explained with reference to likely patterns of accumulation, ablation and vertical compression/extension. The calculated mean annual mass balance of $-0{\cdot}61$ m w.e. a^{-1} is greater than that derived from field measurements over the same time period by the Norsk Polarinstitutt. However, underestimates of field-based mass balance measurements have also been reported elsewhere (Fleming *et al*., 1997; Hagen *et al*., 2000). Part of the discrepancy is probably associated with the difficulties of producing accurate glacier DEMs due to problems of obtaining ground control points in mountainous terrain, and errors in height determination, especially over snow and where shading is common. However, part of the discrepancy may also be associated with using centreline stake measurements to represent the mass balance of large areas. Because of continuing problems inherent in both techniques, it is essential to continue to compare remotely sensed mass balance estimates with field-based measurements.

The bed and surface DEMs have also been used to identify changes in the drainage system structure of the glacier between 1977 and 1995. If subglacial water pressures are high, water is likely to flow at high discharges in a discrete drainage routeway down most of the tongue, and exit the glacier in several hydraulically efficient outlets at the snout. For moderate water pressures, water is likely to flow at moderate discharges in a more dispersed drainage system and water may become ponded at several locations beneath the glacier tongue, emerging in a few hydraulically inefficient outlets at the snout. If water pressures are atmospheric, water will flow at moderate discharges in a highly dispersed drainage system and emerge in one hydraulically inefficient outlet towards the centre of the snout in 1977 or to the east in 1995.

Observations of outlet position during the 1990s suggest that in most years, early summer drainage is established under moderate subglacial water pressures ($P_w \approx 0{\cdot}5P_i$) and water is directed towards the eastern half of the glacier snout. If meteorological and hydrological conditions lead to the development of high subglacial water pressures ($P_w \approx P_i$) during the early summer, water may be directed towards the western half of the snout into a pre-existing conduit. This conduit is likely to be a relic from earlier years when the glacier was bigger and more water was routed at high pressure towards the west. Higher pressures in the past may have been a result of smaller drainage elements in the spring, due to higher winter closure rates when the glacier was bigger and faster moving, or higher spring discharges when more of the glacier was temperate and more water was able to flow subglacially.

Long-term changes in the position of proglacial outlet streams may occur as a result of changes in glacier geometry, but short-term changes may also occur in response to early season water pressures dependent on meteorological and hydrological conditions. This has important implications where subglacial waters are tapped for hydroelectric power generation (Bézinge, 1981; Hantz and Lliboutry, 1983; Hooke *et al*., 1984), or where proglacial streams, especially those susceptible to jökulhlaups, may threaten roads or bridges (Björnsson, 1992). To accurately model subglacial water routing to glacier margins and predict how this might change in the future, it is important to account not only for changes in glacier geometry, but also for variations in meteorology and hydrology and their effects on subglacial water pressures.

Finally, our results suggest that water stored beneath the warm-based core of polythermal glaciers may escape through the cold-based snout via either fissures within sediments beneath a permafrost layer, fractures within basal ice or at the ice bed interface via hydraulic jacking. The conditions giving rise to drainage via these different mechanisms need further investigation on a variety of polythermal glaciers.

ACKNOWLEDGEMENTS

D.R. acknowledges the support of NERC studentship GT04/97/57/FS; St John's College, Cambridge; The Dudley Stamp Memorial Fund (The Royal Society); The Philip Lake Fund (Department of Geography, University of Cambridge); The B.B. Roberts Fund (Scott Polar Research Institute, University of Cambridge); The Tennant Fund (Department of Anglo-Saxon, Norse and Celtic, University of Cambridge); and The Worts Travelling Scholars Fund. A.H. acknowledges the Nuffield Foundation ("NUF-NAL"). Maps and aerial photographs were used with permission from the Norwegian Polar Institute ©. Stuart Lane kindly assisted with the analytical photogrammetry. Thanks to Nick Cox at the NERC Arctic Research Station for logistical support, and to Nathan Rippin, Mark Holdaway, Ruth Jenkins, Elaine Blyth and Angela Morris for help in the field. Thanks also to Paul Mumford for some hydrological observations and Richard Westaway for assistance with various aspects of DEM production. Philip Stickler helped in the production of Figure 1. The comments of two anonymous referees helped to improve this paper.

REFERENCES

Andreassen LM. 1999. Comparing traditional mass balance measurements with long term volume change extracted from topographical maps: A case study of Storbreen Glacier in Jotunheimen, Norway, for the period 1940–1997. *Geografiska Annaler* **81A**: 467–476.

Arnold N, Sharp M. 1992. Influence of glacier hydrology on the dynamics of a large Quaternary ice sheet. *Journal of Quaternary Science* **7**: 109–124.

Beniston M, Diaz HH, Bradley RS. 1997. Climatic change at high elevation sites: an overview. *Climatic Change* **36**: 233–251.

Bézinge A. 1981. Glacial meltwater streams, hydrology and sediment transport: The case of the Grande Dixence hydroelectricity scheme. In *Glacio-fluvial Sediment Transfer*, Gurnell AM, Clark MJ (eds). Wiley: New York; 473–498.

Bindschadler R, Harrison WD, Raymond CF, Crosson R. 1977. Geometry and dynamics of a surge-type glacier. *Journal of Glaciology* **18**(79): 181–194.
Björnsson H. 1982. Drainage basins on Vatnajökull mapped by radio echo sounding. *Nordic Hydrology* **13**: 213–232.
Björnsson H. 1988. *Hydrology of Ice Caps in Volcanic Regions*. Societas Scientarium Islandica, Rit XLV: Reykjavík.
Björnsson H. 1992. Jökulhlaups in Iceland: prediction, characteristics and simulation. *Annals of Glaciology* **16**: 95–106.
Björnsson H. 1998. Hydrological characteristics of the drainage system beneath a surging glacier. *Nature* **395**: 771–774.
Björnsson H, Gjessing Y, Hamran S-E, Hagen JO, Liestøl O, Pálsson F, Erlingsson B. 1996. The thermal regime of sub-polar glaciers mapped by multi-frequency radio-echo sounding. *Journal of Glaciology* **42**(140): 23–32.
Cattle H, Crossley J. 1995. Modelling Arctic climate change. *Philosophical Transactions of the Royal Society of London, Series A* **352**(1699): 201–213.
Clarke GKC, Blake EW. 1991. Geometric and thermal evolution of a surge-type glacier in its quiescent state – Trapridge Glacier, Yukon-Territory, Canada, 1969–89. *Journal of Glaciology* **37**(125): 158–169.
Clarke GKC, Collins SG, Thompson DE. 1984. Flow, thermal structure and subglacial conditions of a surge-type glacier. *Canadian Journal of Earth Science* **21**: 232–240.
Copland L, Sharp M. 2000. Radio-echo sounding determination of polythermal glacier hydrology. In *Eighth International Conference on Ground Penetrating Radar*, Noon D, Stickley GF, Longstaff D (eds). SPIE Vol. **4084**: 59–64.
Denton GH, Hughes TJ (eds) 1981. *The Last Great Ice Sheets*. Wiley: New York.
Dixon LFJ, Barker R, Bray M, Farres P, Hooke J, Inkpen R, Merel A, Payne D, Shelford A. 1998. Analytical photogrammetry for geomorphological research. In *Landform Monitoring, Modelling and Analysis*, Lane SN, Richards KS, Chandler JH (eds). Wiley: Chichester; 63–94.
Dowdeswell JA, Drewry DJ. 1989. The dynamics of Austfonna, Nordaustlandet, Svalbard: surface velocities, mass balance, and subglacial melt water. *Journal of Glaciology* **12**: 37–45.
Dyurgerov MB, Meier MF. 1997. Year-to-year fluctuations of global mass balance of small glaciers and their contribution to sea-level changes. *Arctic and Alpine Research* **29**(4): 392–402.
Etzelmüller B, Vatne G, Ødegård RS, Sollid JL. 1993. Mass balance changes of surface slope, crevasse and flow pattern of Erikbreen, northern Spitsbergen: an application of a geographical information system. *Polar Research* **12**(2): 131–146.
Fleming KM, Dowdeswell JA, Oerlemans J. 1997. Modelling the mass balance of northwest Spitsbergen glaciers and responses to climate change. *Annals of Glaciology* **24**: 203–210.
Flowers GE, Clarke GKC. 1999. Surface and bed topography of Trapridge Glacier, Yukon Territory, Canada: digital elevation models and derived hydraulic geometry. *Journal of Glaciology* **45**(149): 165–174.
Fountain AG. 1993. Geometry and flow conditions of subglacial water at South Cascade Glacier, Washington State, U.S.A.; an analysis of tracer injections. *Journal of Glaciology* **39**(131): 143–156.
Fountain AG, Vaughn BH. 1995. Changing drainage patterns within South Cascade Glacier, Washington, USA, 1964–1992. *International Association of Hydrological Sciences Publication,* No. **228**: 379–386.
Fountain AG, Walder JS. 1998. Water flow through temperate glaciers. *Review of Geophysics* **36**(3): 299–328.
Glasser NF, Hambrey MJ. 2001. Styles of sedimentation beneath Svalbard valley glaciers under changing dynamic and thermal regime. *Journal of Geological Society* **158**: 697–707.
Hagen JO, Liestøl O. 1990. Long-term glacier mass-balance investigations in Svalbard. *Annals of Glaciology* **14**: 102–106.
Hagen JO, Sætrang A. 1991. Radio-echo soundings of sub-polar glaciers with low-frequency radar. *Polar Research* **9**(1): 99–107.
Hagen JO, Korsen OM, Vatne G. 1991. Drainage pattern in a subpolar glacier: Brøggerbreen, Svalbard. In *Arctic Hydrology, Present and Future Tasks*, Gjessing Y, Hagen JO, Hassel KA, Sand K, Wold B (eds). Norwegian National Committee for Hydrology: 121–131.
Hagen JO, Etzelmüller B, Nuttall A-M. 2000. Runoff and drainage pattern derived from digital elevation models, Finsterwalderbreen, Svalbard. *Annals of Glaciology* **31**: 147–152.
Hansen S. 1999. *A photogrammetrical, climate-statistical and geomorphological approach to the post Little Ice Age changes of the Midre Lovénbreen glacier, Svalbard*. Masters thesis, University of Copenhagen.
Hanson B. 1995. A fully three-dimensional finite-element model applied to velocities on Storglaciären, Sweden. *Journal of Glaciology* **41**(137): 91–102.
Hanssen-Bauer I, Kristensen Solas M, Steffensen EL. 1990. *The climate of Spitsbergen* Norsk Meteorologisk Institutt Report No. 39/90: Oslo.
Hantz D, Lliboutry L. 1983. Waterways, ice permeability at depth and water pressures at Glacier d'Argentière, French Alps. *Journal of Glaciology* **29**: 227–239.
Heine JT, McTigue DF. 1996. A case for cold-based continental ice sheets – a transient thermal model. *Journal of Glaciology* **42**: 37–42.
Heinrichs TA, Mayo LR, Echelmeyer KA, Harrison WD. 1996. Quiescent-phase evolution of a surge-type glacier: Black Rapids Glacier, Alaska, USA. *Journal of Glaciology* **42**(140): 110–122.
Hodgkins R. 1994. *The seasonal evolution of meltwater discharge, quality and routing at a High-Arctic glacier*. PhD thesis, Scott Polar Research Institute, University of Cambridge.
Hodgkins R. 1997. Glacier hydrology in Svalbard, Norwegian High Arctic. *Quaternary Science Reviews* **16**: 957–973.
Hodson AJ, Ferguson RI. 1999. Fluvial suspended sediment transport from cold and warm-based glaciers in Svalbard. *Earth Surface Processes and Landforms* **24**: 957–974.
Hodson A, Tranter M, Vatne G. 2000. Contemporary rates of chemical denudation and atmospheric CO_2 sequestration in glacier basins: an Arctic perspective. *Earth Surface Processes and Landforms* **25**: 1447–1471.
Holmlund P. 1988. Internal geometry and evolution of moulins, Storglaciären, Sweden. *Journal of Glaciology* **34**(117): 242–248.
Hooke RL. 1984. On the role of mechanical energy in maintaining subglacial water conduits at atmospheric pressure. *Journal of Glaciology* **30**(105): 180–187.
Hooke RL. 1989. Englacial and subglacial hydrology – A qualitative review. *Arctic and Alpine Research* **21**(3): 221–233.
Hooke RL, Wold B, Hagen JO. 1984. Subglacial hydrology and sediment transport at Bondhusbreen, southwest Norway. *Geological Society of America Bulletin* **96**: 388–397.

Houghton JT, Ding Y, Griggs DJ, Noguer M, van den Linden PJ, Dai X, Maskell K, Johnson CA. 2001. *Climate Change 2001: The Scientific Basis*. Cambridge University Press: Cambridge.
Hubbard A, Blatter H, Nienow P, Mair D, Hubbard B. 1998. Comparison of a three-dimensional model for glacier flow with field data from Haut Glacier d'Arolla, Switzerland. *Journal of Glaciology* **44**(147): 368–378.
Hubbard A, Willis I, Sharp M, Mair D, Nienow P, Hubbard B, Blatter H. 2000. Glacier mass-balance determined by remote sensing and high-resolution modelling. *Journal of Glaciology* **46**(154): 491–498.
Hubbard B, Nienow P. 1997. Alpine subglacial hydrology. *Quaternary Science Reviews* **16**: 939–955.
IAHS/UNEP/UNESCO. 1993. *Fluctuations of glacier 1985–1990,* Volume VI. World Glacier Monitoring Service: Zurich.
IAHS/UNESCO. 1998. *Fluctuations of glacier 1990–1995,* Volume VII. World Glacier Monitoring Service: Zurich.
Iken A. 1981. The effect of the subglacial water pressure on the sliding velocity of a glacier in an idealized numerical model. *Journal of Glaciology* **27**(97): 407–421.
Iken A, Truffer M. 1997. The relationship between subglacial water pressure and velocity of Findelengletscher, Switzerland, during its advance and retreat. *Journal of Glaciology* **43**(144): 328–338.
Jiskoot H, Murray T, Boyle P. 2000. Controls on the distribution of surge-type glaciers in Svalbard. *Journal of Glaciology* **46**(154): 412–422.
Kaab A, Funk M. 1999. Modelling mass balance using photogrammetric and geophysical data: a pilot study at Griesgletscher, Swiss Alps. *Journal of Glaciology* **45**(151): 575–583.
Kamb B, Raymond CF, Harrison WD, Engelhardt H, Echelmeyer KA, Humphrey N, Brugman MM, Pfeffer T. 1985. Glacier surge mechanism: 1982–1983 surge of Variegated Glacier, Alaska. *Science* **227**(4686): 469–479.
Krawczyk WE. 1992. Chemical characteristics of water circulating in the Werenskiold glacier (south-west Spitzbergen). *Proceedings of the 2nd International Symposium of Glacier Caves and Karst in Polar Regions*, Silesian University, Sosnowiec: 65–80.
Lefauconnier B, Hagen JO, Ørbæk JB, Melvold K, Isaksson E. 1999. Glacier balance trends in the Kongsfjorden area, western Spitsbergen, Svalbard, in relation to the climate. *Polar Research* **18**(2): 307–313.
Liestøl O. 1977. Pingos, springs and permafrost in Spitsbergen. *Norsk Polarinstitutt Årbok* **1975**: 7–29.
Lliboutry L. 1968. General theory of subglacial cavitation and sliding of temperate glaciers. *Journal of Glaciology* **7**(49): 21–58.
Nienow P, Sharp M, Willis I. 1998. Seasonal changes in the morphology of the subglacial drainage system, Haut Glacier d'Arolla, Switzerland. *Earth Surface Processes and Landforms* **23**(9): 825–843.
Nye JF. 1957. The distribution of stress and velocity in glaciers and ice sheets. *Proceedings of the Royal Society of London, Series A* **239**: 113–133.
Ødegård RS, Hamran S-E, Bø PH, Etzelmüller B, Vatne G, Sollid JL. 1992. Thermal regime of a valley glacier, Erikbreen, Northern Spitsbergen. *Polar Research* **11**(2): 69–79.
Pfeffer WT, Bretherton CS. 1987. The effect of crevasses on the solar heating of a glacier surface. *The Physical Basis of Ice Sheet Modelling (Proceedings of the Vancouver Symposium, August 1987)*. IAHS Publication **170**: 191–205.
Reinhardt W, Rentsch H. 1986. Determination of changes in volume and elevation of glaciers using digital elevation models from the Veragtferner, Ötztal Alps, Austria. *Annals of Glaciology* **8**: 151–155.
Röthlisberger H, Lang H. 1987. Glacial hydrology. In *Glacio-Fluvial Sediment Transfer: An Alpine Perspective*, Gurnell AM, Clarke MJ (eds). Wiley: London; 207–284.
Sharp M, Richards K, Willis I, Arnold N, Nienow P, Lawson W, Tison J-L. 1993. Geometry, bed topography and drainage system structure of the Haut Glacier D'Arolla, Switzerland. *Earth Surface Processes and Landforms* **18**: 557–571.
Shreve RL. 1972. Movement of water in glaciers. *Journal of Glaciology* **11**(62): 205–214.
Skidmore ML, Sharp MJ. 1999. Drainage system behaviour of a high-Arctic polythermal glacier. *Annals of Glaciology* **28**: 209–215.
Stone DB, Clarke GKC. 1996. *In situ* measurements of basal water quality and pressure as an indicator of the character of subglacial drainage systems. *Hydrological Processes* **10**: 615–628.
Stouffer RJ, Manabe S, Bryan K. 1989. Interhemispheric asymmetry in climate response to a gradual increase of atmospheric carbon dioxide. *Nature* **342**(6250): 660–662.
Sugden DE. 1977. Reconstruction of the morphology, dynamics and thermal characteristics of the Laurentide ice sheet at its maximum. *Arctic and Alpine Research* **9**: 21–47.
Tranter M, Brown GH, Hodson AJ, Gurnell AM. 1996. Hydrochemistry as an indicator of subglacial drainage system structure: a comparison of alpine and sub-polar environments. *Hydrological Processes* **10**: 541–556.
Wadham JL, Hodson AJ, Tranter M, Dowdeswell JA. 1998. The hydrochemistry of meltwaters draining a polythermal-based high Arctic glacier, south Svalbard: I. The ablation season. *Hydrological Processes* **12**: 1825–1849.
Wadham JL, Tranter M, Dowdeswell JA. 2000. Hydrochemistry of meltwaters draining a polythermal-based high-Arctic glacier, south Svalbard: II. Winter and early Spring. *Hydrological Processes* **14**: 1767–1786.
Walsh JE. 1991. The Arctic as a bellwether. *Nature* **352**(6330): 19–20.
Willis IC, Arnold N, Sharp M, Bonvin J-L, Hubbard B. 1998. Mass balance and flow variations of Haut Glacier d'Arolla, Switzerland calculated using digital terrain modelling techniques. In *Landform Modelling, Monitoring and Analysis*, Lane SN, Chandler JH, Richards KS (eds). Wiley: Chichester; 343–362.

